iScience

CellPress
OPEN ACCESS

Article

# A physiologically based model of bile acid metabolism in mice

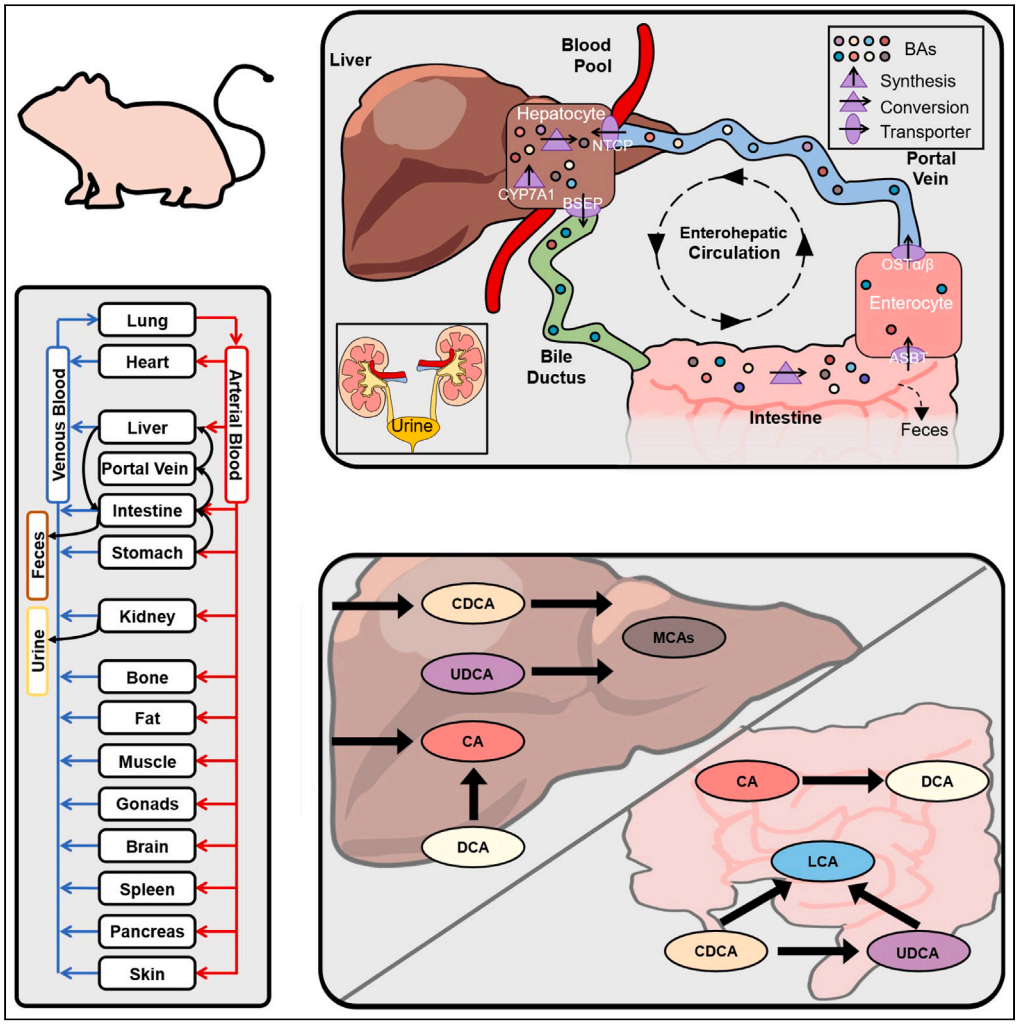


Bastian Kister, Alina Viehof, Ulrike Rolle-Kampczyk, ..., Martin von Bergen, Thomas Clavel, Lars Kuepfer

lkuepfer@ukaachen.de

## Highlights

A mechanistic computational model of bile acid metabolism in mice was developed

Sex specificity in bile acid metabolism is taken into account

The model can be used for simulation of disease-related alterations

Study design within a 3R context is supported by the model

Kister et al., iScience *26*, 107922
October 20, 2023 
https://doi.org/10.1016/j.isci.2023.107922

iScience

CellPress
OPEN ACCESS

Article

# A physiologically based model of bile acid metabolism in mice

Bastian Kister,[1,2] Alina Viehof,[3] Ulrike Rolle-Kampczyk,[4] Annika Schwentker,[5] Nicole Simone Treichel,[3] Susan A.V. Jennings,[3] Theresa H. Wirtz,[6] Lars M. Blank,[2] Mathias W. Hornef,[5] Martin von Bergen,[4,7,8] Thomas Clavel,[3] and Lars Kuepfer[1,9,*]

## SUMMARY

**Bile acid (BA) metabolism is a complex system that includes a wide variety of primary and secondary, as well as conjugated and unconjugated BAs that undergo continuous enterohepatic circulation (EHC). Alterations in both composition and dynamics of BAs have been associated with various diseases. However, a mechanistic understanding of the relationship between altered BA metabolism and related diseases is lacking. Computational modeling may support functional analyses of the physiological processes involved in the EHC of BAs along the gut-liver axis. In this study, we developed a physiologically based model of murine BA metabolism describing synthesis, hepatic and microbial transformations, systemic distribution, excretion, and EHC of BAs at the whole-body level. For model development, BA metabolism of specific pathogen-free (SPF) mice was characterized *in vivo* by measuring BA levels and composition in various organs, expression of transporters along the gut, and cecal microbiota composition. We found significantly different BA levels between male and female mice that could only be explained by adjusted expression of the hepatic enzymes and transporters in the model. Of note, this finding was in agreement with experimental observations. The model for SPF mice could also describe equivalent experimental data in germ-free mice by specifically switching off microbial activity in the intestine. The here presented model can therefore facilitate and guide functional analyses of BA metabolism in mice, e.g., the effect of pathophysiological alterations on BA metabolism and translation of results from mouse studies to a clinically relevant context through cross-species extrapolation.**

## INTRODUCTION

Bile acids (BAs) are involved in many physiological processes in the body including digestion of nutrients or hormone metabolism.[1,2] The bile acid (BA) pool is a complex mixture of different BA species. Primary BAs are synthesized from cholesterol in the liver and are converted to various secondary BAs by the intestinal microbiome.[3] Bile acid synthesis involves several enzymes located in different cellular compartments such as the cytosol, endoplasmic reticulum, mitochondria, and peroxisomes. The process is intricate and can be classified into two significant pathways: the classic (neutral) pathway and the alternative (acidic) pathway. Most of the bile acids in humans and mice are produced through the classic pathway,[4] which modifies the sterol nucleus of cholesterol before oxidatively cleaving its side chain. The alternative pathway starts with an initial hydroxylation on the side chain of cholesterol, followed by 7α-hydroxylation of the sterol nucleus. Microbial transformation of bile acids occurs mainly in the distal portion of the small intestine and large intestine, resulting in the production of secondary bile acids through several reaction pathways such as deconjugation, dehydrogenation, dihydroxylation, and epimerization.[5,6] Bile acid 7-dehydroxylating bacteria lead to the production of 7-dehydroxylated secondary bile acids, including DCA and LCA that are primary constituents of secondary bile acids, especially in feces.[7] In mice, gut microbiota mainly produces ω-MCA as the β-MCA metabolite.[8] Both primary and secondary BAs are furthermore conjugated with either glycine or taurine in hepatocytes.

Within the body, BAs continuously undergo enterohepatic circulation (EHC) between the liver and the intestine. Hepatic BAs are secreted into the bile canaliculi and accumulate in the gallbladder. Upon food intake, gallbladder contractions release large amounts of the stored BAs

[1]Institute for Systems Medicine with Focus on Organ Interaction, University Hospital RWTH Aachen, Aachen, Germany
[2]Institute of Applied Microbiology - iAMB, Aachen Biology and Biotechnology - ABBt, RWTH Aachen University, Aachen, Germany
[3]Functional Microbiome Research Group, Institute of Medical Microbiology, University Hospital RWTH Aachen, Aachen, Germany
[4]Department of Molecular Systems Biology, Helmholtz Centre for Environmental Research (UFZ), Leipzig, Germany
[5]Institute of Medical Microbiology, University Hospital RWTH Aachen, Aachen, Germany
[6]Department of Medicine III, University Hospital RWTH Aachen, Aachen, Germany
[7]German Centre for Integrative Biodiversity Research (iDiv) Halle-Jena-Leipzig, Leipzig, Germany
[8]Faculty of Life Sciences, Institute of Biochemistry, University of Leipzig, Leipzig, Germany
[9]Lead contact
*Correspondence: lkuepfer@ukaachen.de
https://doi.org/10.1016/j.isci.2023.107922

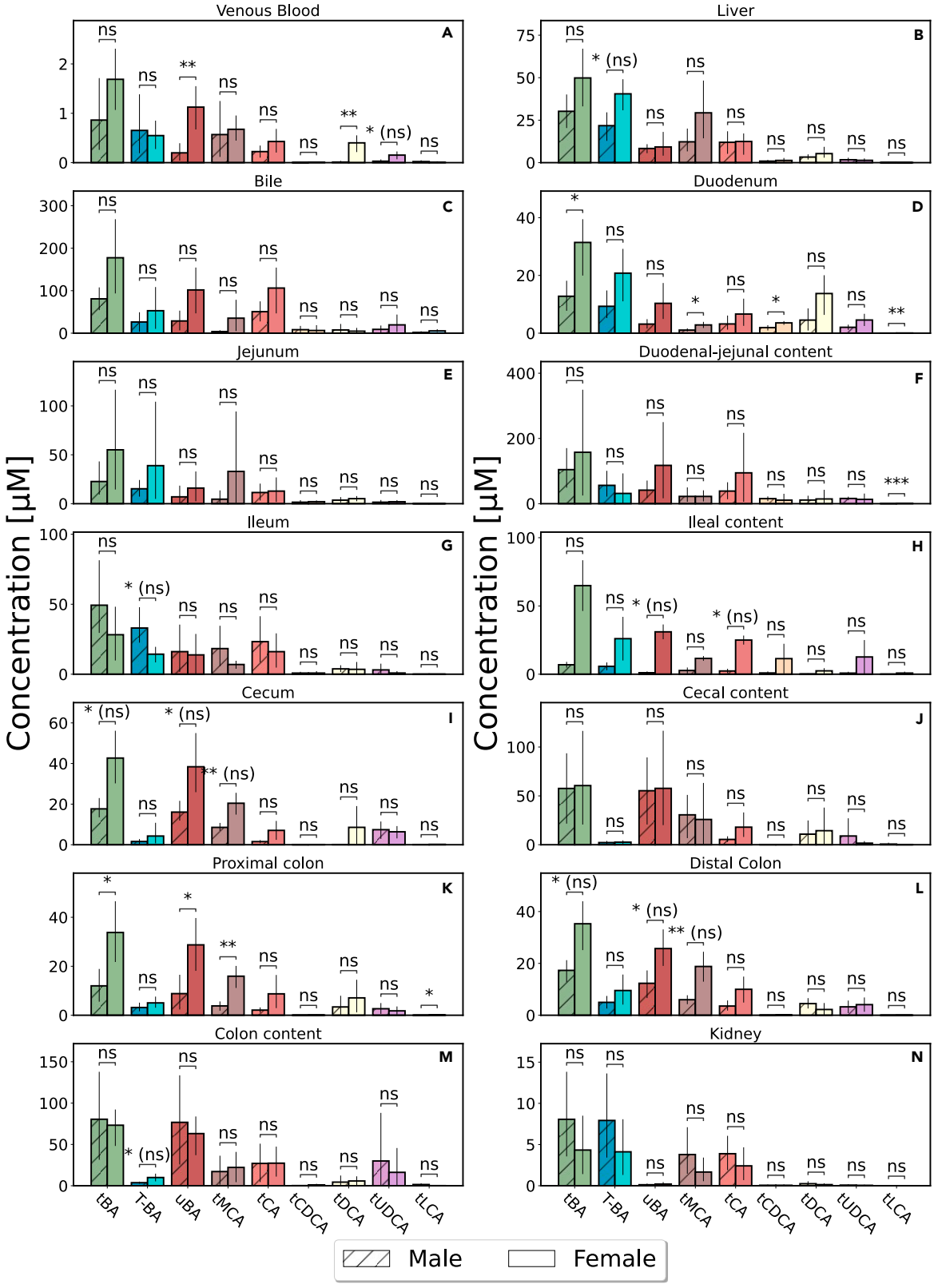
Venous Blood
A
Liver
B
Bile
C
Duodenum
D
Jejunum
E
Duodenal-jejunal content
F
Ileum
G
Ileal content
H
Cecum
I
Cecal content
J
Proximal colon
K
Distal Colon
L
Colon content
M
Kidney
N
Concentration [µM]
Concentration [µM]
tBA
T-BA
uBA
tMCA
tCA
tCDCA
tDCA
tUDCA
tLCA
Male
Female

**Figure 1. Bile acid levels in SPF mice**

Concentration of total BAs (tBA), tauro-conjugated BAs (T-BA), unconjugated BA (uBA), total cholic acid (tCA), total muricholic acids (tMCA), total chenodeoxycholic acid (tCDCA), total deoxycholic acid (tDCA), total ursodeoxycholic acid (tUDCA), and total lithocholic acid (tLCA) in various organs and samples from male (striped bars) and female SPF mice (open bars). Samples were taken from venous blood plasma (A), liver tissue (B), bile (C), tissue of the duodenum (D), jejunum (E), ileum (G), cecum (I), proximal and distal colon (K and L) and corresponding contents of these gut segments (F, H, J, M) and kidney (N). Statistical differences were assessed by independent t test. Statistical significance is marked with asterisks and (ns) indicates nonsignificance after correction for multiple testing using Benjamini-Hochberg correction. Error bars represent the standard deviation.

into the small intestine to facilitate lipid absorption. BAs are further transported along the gut. Starting already within the small intestine but especially within the colon, BAs are subject to microbial transformations such as deconjugation and the production of secondary BAs, e.g., by dehydrogenation. Most BAs are actively taken up by enterocytes, predominantly in the ileum, and further excreted toward portal blood. The remaining BAs are then either taken up by passive diffusion or they are secreted with the feces. From the portal blood, BAs are efficiently reabsorbed into the liver. Through sinusoidal transport they may subsequently reach the vascular circulation and eventually other tissues.

Due to the systemic nature of BA metabolism, diseases of both the liver (e.g., liver cirrhosis, liver cancer, or inflammatory bowel disease) and the intestine (e.g., ulcerative colitis or Crohn disease) have been associated with alterations in BA composition and distribution.[2,9–16] Such changes, however, may be difficult to investigate due to the complexity of the physiological processes involved and invasive sampling techniques required.

In this work, we developed a physiologically based (PBPK) model of murine BA metabolism at the whole-body level that may be used as a platform for mechanistic investigation of BA metabolism. This model is of particular interest because mice are the most commonly used animal model to investigate human metabolism.[17,18] Mice produce cholic acid (CA) as well as muricholic acids (MCAs) that are made from chenodeoxycholic acid (CDCA). MCAs are hydroxylated at the C-6 position, which alters their physicochemical as well as the signaling properties. MCAs are more hydrophilic and less cytotoxic than other BAs and function as FXR antagonists instead of activating FXR signaling like other BAs.[19] Among others, this complicates translation of insights generated in mouse experiments to what can be expected in humans.

Our model describes the physiology of murine BA metabolism in great detail and can be used to simulate tissue concentration profiles of the most abundant BAs in mice. To inform the model, mice were experimentally characterized concerning their BA composition in various organs as well as their BA transporter expression along the gut axis and their cecal microbiota. Our model was further validated with complementary datasets generated from germ-free mice. The here presented model can be used to simulate BA levels in tissues that are experimentally inaccessible. Likewise, it can be used to analyze the effect of pathophysiological alterations on BA metabolism. The model may hence serve as a tool for hypothesis testing and as a bridge between discoveries within mouse studies and clinical applications in human patients.

## RESULTS

### A physiologically based model of bile acid metabolism

The physiologically based murine model of BA metabolism includes synthesis, hepatic and microbial transformations, (re-)circulation, and excretion of BAs. For model development we used a PBPK model[20] in which BA metabolites were considered as the circulating molecules. The basic PBPK model represents the physiology of mice at a large level of detail. It therefore includes a significant amount of prior physiological knowledge regarding organ volumes, tissue composition, organ surface areas, or blood perfusion rates.[21,22] Of note, the extrapolation to new scenarios and conditions is well possible due to the mechanistic structure of the underlying PBPK model.[21,23]

In order to specifically inform physiological and kinetic parameters for bile acid metabolism in mice, extensive experimental data were collected. This dataset comprised measurements of BA levels and composition in different tissues of specific pathogen-free (SPF) mice (Figure 1), physiological parameters (Figure 2), quantification of transporter gene expression in different segments of the gut, as well as cecal microbiome diversity and composition (Figure 3).

An initial screening of BA levels showed that female mice had in general higher levels of BAs than their male littermates, which is in agreement with published studies.[24] In our data, total BA concentration in female mice was consistently increased in venous blood serum, liver, bile, and intestinal tissues (Figures 1A–1E, 1I, 1K, and 1L). Levels in the gut lumen were higher in the small intestine (Figures 1F and 1H), whereas the content of the large intestine did not show a clear picture (Figures 1J and 1M). Only in the ileal tissue, male mice displayed higher concentration of BAs than female mice (Figure 1G). Concentration of primary BA in gallbladder bile was consistently elevated in female mice but sex differences do not amount to statistical significance (Figure S2).

In order to account for sex-related variation in BA metabolism, we built separate physiologically based models for male and female SPF mice. Using physiologically based modeling to describe bile acid metabolism enabled us to incorporate explicit information on the organism's physiology (Figure 2). In this study, male mice were approximately 30% heavier (Figure 2A), and correspondingly in female mice the liver and kidney were smaller (Figure 2C). Interestingly, the intestine had approximately the same length regardless of sex; thus, female mice showed a longer intestine in relation to their body weight (Figure 2B).

Four transport processes were considered in the model: (1) excretion of BAs from the liver into the duodenum by the bile salt export pump (BSEP), (2) uptake from the gut lumen by the apical sodium-dependent bile acid transporter (ASBT), (3) excretion from enterocytes to portal blood by the organic solute and steroid transporter (OST $\alpha/\beta$), and (4) uptake of BAs from portal blood into hepatocytes by the sodium/taurocholate cotransporting polypeptide (NTCP). Expression of the transporters (ASBT, OST $\alpha/\beta$) along the gut axis showed overall no

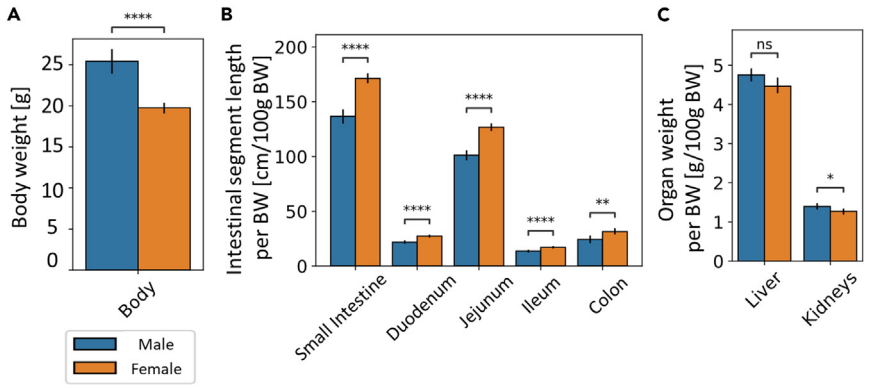


**Figure 2. Physiological differences between male and female mice**

(A–C) Assessment of sex-related differences in body weight (A), length of intestinal segments (B) as well as weight of the liver and the kidneys (C) in SPF mice (male [blue bars], female [orange bars]). Significant differences were tested by two-way, independent t test, and significance was marked with asterisks. Error bars represent the standard deviation.

differences between male and female mice; however, they varied strongly between different gut segments (Figure 3A). Overall, expression of these transporters was limited to the liver (NTCP and BSEP) and the intestine (ASBT, OST $\alpha/\beta$) in the model.

To examine potential differences in the microbiota of male and female mice, the microbial diversity and composition within the cecum were analyzed. First, we determined α-diversity for within-sample differences. Species richness and Shannon effective counts showed no significant sex-related difference (Figure 3B). Similarities in microbial community structure (β-diversity) were assessed based on generalized UniFrac distances.[25,26] We observed no statistically significant separation of mice based on sex and an overall high similarity between all samples (Figure 3C, p-value=0.105).

Significant differences between male and female mice were observed at the level of bacterial composition. In female mice, the family of *Lactobacillaceae* was more abundant, whereas an unknown genus within the family *Muribaculaceae* was more prominent in male mice (Figure 3D). Although various *Lactobacillaceae* species are able to metabolize BAs,[27] the observed difference in relative abundance between male and female mice was only significant without p value adjustment and overall, rather low. For the other significantly abundant genus, no information is available linking it to BA metabolism. Overall, these results indicate that there were no major differences in intestinal transporter expression and microbiota diversity and composition between male and female mice in this study.

Besides the aforementioned physiology of the organism, physicochemical properties such as molecular weight, solubility, lipophilicity (logP), and plasma-protein binding (fraction unbound) are a second important pillar of PBPK models.[20] Organ-plasma partitioning and passive transport can be directly derived from these parameters using an appropriate distribution model. For the physiologically based model of bile acid metabolism, physicochemical properties of the tauro-conjugated forms (Table 1) were used to inform the compound properties of the PBPK model for small molecules.

In the computational model, total levels of CA, MCAs, CDCA, DCA, UDCA, and LCA were considered as these represent the most abundant BAs that could also be measured in all compartments. *De novo* synthesis of BAs was considered as a constant formation rate in the intracellular space of the liver, and its magnitude was estimated from the excretion rate in feces[31–33] and urine.[34] Both excretion processes were considered by passive transport or active clearance, respectively. Subsequent formation of MCA using CDCA or UDCA as well as hepatic DCA hydroxylation was included in the model. Microbial metabolism of BAs was modeled as net enzymatic reactions, and the relative abundance of the corresponding enzymes along the gut was correlated with the activity of bile salt hydrolase (BSH).[35] The included reactions were dehydroxylation of CA to DCA and CDCA and UDCA to LCA as well as epimerization of CDCA to UDCA. A schematic overview of the model structure is shown in Figure S1.

## Model calibration to data from SPF mice

For parameter estimation, we allowed sex-related differences in active hepatic processes. It was found that downregulation of BA synthesis and the transporter NTCP is both necessary and sufficient to explain BA composition and levels in male and female SPF mice (data not shown). This agrees with earlier findings showing upregulation of BA synthesis (*Cyp7a1, Cyp27a1*)[36] as well as an elevated expression of the basolateral uptake transporter NTCP in female mice.[37] This striking agreement with earlier findings is the first indication of the predictive capabilities of the computational model and generates confidence for further analyses.

Following parameter estimation (fitted parameters shown in Tables S1–S3), the final model adequately described experimentally measured BA levels in various organs, in both male and female SPF mice (Figures 4A, 4B, and S3). Up to 60% of the experimental data were recapitulated within one standard deviation (SD), 92% within a 2-fold SD, and only 12 of 156 data points deviated by more than 2 SDs (Figures 4C and 4D). Even though the model describes a complex system and the measured data showed high variation, especially in the intestine, a good agreement between experimental data and model simulations was achieved.

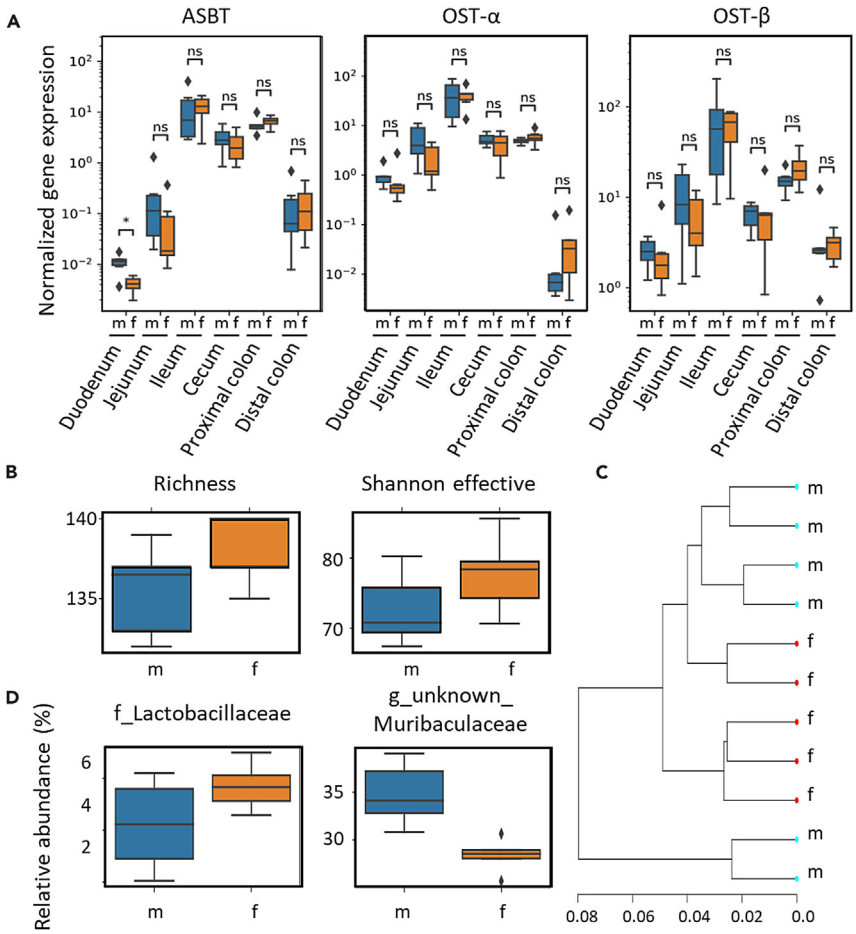


**Figure 3. Sex-related differences in intestinal BA metabolism**

Assessment of sex-related differences in the intestine relevant to BA metabolism.

(A) Expression of the BA transporters ASBT, OST-α, and OST-β (from left to right) along the gut axis in male and female SPF mice measured by qPCR. Statistical significance was assessed by Mann-Whitney U-test, and statistical significance is marked with asterisks (male [blue bars], female [orange bars]).

(B and C) Analysis of the cecal microbiota in male and female SPF mice by assessing the number of observed species (richness) and effective Shannon counts as measures of α-diversity and (C) β-diversity by hierarchical clustering of samples based on Generalized UniFrac distances.

(D) Relative abundance of the family of *Lactobacillaceae* and an unknown genus within *Muribaculaceae*, which significantly differed between male and female mice. Statistical significance was determined using Kruskal-Wallis and Wilcoxon rank-sum test ($\alpha = 0.05$).

To assess model behavior, a sensitivity analysis was performed determining the influence of the fitted parameters on various BA concentrations also measured experimentally (Tables S4–S12). All assessed BA levels were affected by changes in BA synthesis. Varying BSEP activity had strongest effects in liver and intestinal content. ASBT parameters influenced all BA species concentration mainly in the intestine, but ASBT parameters specific for secondary BA affected the corresponding concentration of the secondary BA beyond the gut. Transport through OST(α/β) controlled most strongly BA levels in intestinal tissues but coefficients were below the chosen threshold (data not shown). Concentrations of BA in venous blood plasma and kidney were sensitive to both BA uptake from portal blood through NTCP and excretion via urine. In summary, the sensitivity analysis showed that BA levels were most affected by parameters of reactions that occur in the same compartment as the observed concentration, with the exception of secondary BA being sensitive to ASBT activity throughout the body. As secondary BA are only produced by microbial action in the intestinal lumen, ASBT-meditated uptake from the luminal space represents the main source of secondary BA for the rest of the body. Overall sensitivity coefficients of all model parameters showed high correlation between both models. Few differential sensitivities could be observed; however, corresponding parameters were without physiological relevance (Figure S4).

## Model qualification to germ-free mice

Due to its mechanistic structure, the physiologically based computational model of murine bile acid metabolism enabled the consideration of new scenarios. To validate the computational model of SPF mice, we next predicted BA levels in germ-free (GF) mice (Figure S5). In the first step,

**Table 1. Physicochemical properties of bile acids used**

| BA species | Property | Value | Source |
|---|---|---|---|
| tCA | MW [g/mol] | 515.7 | PubChem Identifier: CID 6675 |
| tCA | Solubility [g/l] | 0.077 | ALOGPS (HMDB,[28]) |
| tCA | logP | 0 | Heuman et al.[29] |
| tCA | pKa (acidic) | −0.88 | ChemAxon (HMDB,[28]) |
| tCA | pKa (basic) | −0.053 | ChemAxon (HMDB,[28]) |
| tCA | FU | 0.359 | Predicted[30] |
| tCDCA | MW [g/mol] | 499.7 | PubChem Identifier: CID 387316 |
| tCDCA | Solubility [g/l] | 0.00748 | ALOGPS (HMDB,[28]) |
| tCDCA | logP | 0.46 | Heuman et al.[29] |
| tCDCA | pKa (acidic) | −0.99 | ChemAxon (HMDB,[28]) |
| tCDCA | pKa (basic) | 0.18 | ChemAxon (HMDB,[28]) |
| tCDCA | FU | 0.0776 | Predicted[30] |
| tUDCA | MW [g/mol] | 499.7 | PubChem Identifier: CID 9848818 |
| tUDCA | Solubility [g/l] | 0.0075 | ALOGPS (HMDB,[28]) |
| tUDCA | logP | −0.94 | Heuman et al.[29] |
| tUDCA | pKa (acidic) | −0.99 | ChemAxon (HMDB,[28]) |
| tUDCA | pKa (basic) | 0.18 | ChemAxon (HMDB,[28]) |
| tUDCA | FU | 0.0776 | Predicted[30] |
| tDCA | MW [g/mol] | 499.7 | PubChem Identifier: CID 2733768 |
| tDCA | Solubility [g/l] | 0.0078 | ALOGPS (HMDB,[28]) |
| tDCA | logP | 0.59 | Heuman et al.[29] |
| tDCA | pKa (acidic) | −0.75 | ChemAxon (HMDB,[28]) |
| tDCA | pKa (basic) | −0.2 | ChemAxon (HMDB,[28]) |
| tDCA | FU | 0.0768 | Predicted[30] |
| tLCA | MW [g/mol] | 483.7 | PubChem Identifier: CID 439763 |
| tLCA | Solubility [g/l] | 0.00028 | ALOGPS (HMDB,[28]) |
| tLCA | logP | 1 | Heuman et al.[29] |
| tLCA | pKa (acidic) | −0.63 | ChemAxon (HMDB,[28]) |
| tLCA | pKa (basic) | −1.1 | ChemAxon (HMDB,[28]) |
| tLCA | FU | 0.0618 | Predicted[30] |
| tMCA | MW [g/mol] | 515.7 | PubChem Identifier: CID 168408 |
| tMCA | Solubility [g/l] | 0.075 | ALOGPS (HMDB,[28]) |
| tMCA | logP | −0.81 | Heuman et al.[29] |
| tMCA | pKa (acidic) | −0.98 | ChemAxon (HMDB,[28]) |
| tMCA | pkA (basic) | 0.084 | ChemAxon (HMDB,[28]) |
| tMCA | FU | 0.365 | Predicted[30] |

Overview of physicochemical properties and their source that were used to inform compound-specific parameters in the PBPK model. For the total BA (total CA: tCA, total CDCA: tCDCA, total UDCA: tUDCA, total DCA: tDCA, total LCA: tLCA, total MCAs: tMCA) the corresponding physicochemical values of the tauro-conjugated form (T-BA) were taken.

any microbial reaction in the SPF model was therefore removed, i.e., the corresponding rate was set to zero. Resulting predictions recapitulated BA concentration in male and female GF mice reasonably well (Figures 5A and S8): about 59% of predicted concentrations fell within one standard deviation, 80% within a 2-fold variation, and 15% predicted BA levels differed more strongly from the measured values (Figures 5B and S8).

In the next step, we aimed to verify whether the inclusion of additional information about the physiology and intestinal transporter expression (Figures S6 and S7) for GF mice would further improve the agreement between model simulations and experimentally measured BA concentrations. This extended model version including the additional information was at first compared against the model variant with no enzymatic activity in the microbiome (Figures 5A and S8). By doing so, model predictions worsened slightly. Less predictions could be

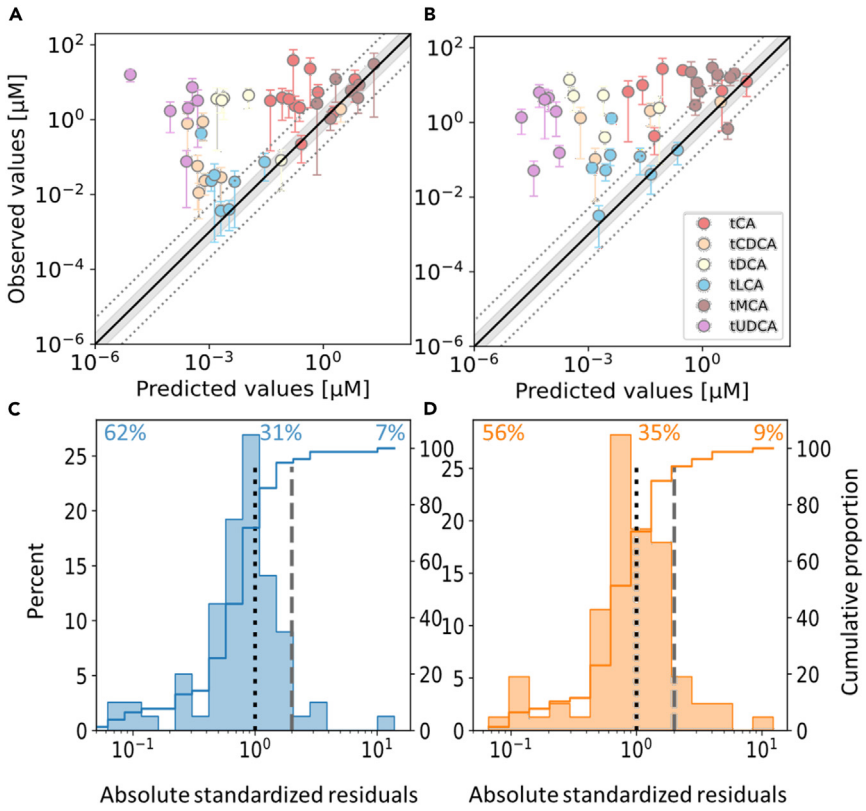


**Figure 4. Model fit to data from SPF mice**

(A–D) Model simulations of bile acid concentration in male (A) and female mice (B) against corresponding data points used for fitting. Only data points with a coefficient of variation below 1 are shown. Unity is represented by a solid black line and a 2- and 5-fold range between predicted and observed values is indicated as a gray area or with dotted lines, respectively. Error bars represent the standard deviation. Distribution of the absolute standardized residuals between model simulations and data of male (C) and female (D) mice (histogram) and the corresponding cumulative function (line). The dotted and dashed lines indicate differences between model simulation and measured data of one SD and two SD, respectively. Cumulative proportions of predictions that are within one SD (top left, residuals left of dotted line), between one and two SD (top middle, residuals between dotted and dashed line), and above two SD (top right, residuals right of dashed line) of measured data are stated at the top of the panel. See also Figure S3.

recapitulated within one SD, but 80% were still within two SDs (Figure 6A), indicating that there are additional differences in BA metabolism between SPF and GF mice.

In the second model variant, expression of the synthesizing enzymes CYP7A1, CYP27A1, and CYP7B1 were increased according to earlier measurements in GF mice.[38–40] However, increasing BA synthesis only yielded better model predictions by also allowing for differential regulation of other hepatic enzymes and processes. Upregulation of BSEP and downregulation of NTCP and MCA production from CDCA improved predictions only slightly (Figure 6B). In the third model variant, BA synthesis was allowed to decrease, and hepatic processes were assumed to be differently regulated. Thus, the most accurate predictions of BA levels in GF mice were obtained, with 59% of predicted concentrations being within one SD, more than 80% being within two SDs, and only 12% that are not explained well.

## Model analyses

After model calibration and validation, the here developed computational model described BA metabolism in both male and female mice with good agreement. The model could hence be applied for comprehensive characterizations of the distribution and composition of BAs throughout the body (Figure 7). Model simulations showed highest BA levels within SI tissue, liver, as well as intestinal lumen. Considerable BA amounts were also predicted within muscle of female mice but not in male mice (Figures 7A and S9). Such relatively high BA levels in non-EHC tissues are due to rather large plasma and interstitial compartments in these organs where intracellular accumulation occurs through passive diffusion from the interstitial compartment. Of note, redistribution may be additionally hampered due to a decrease in intracellular pH. The BA pool was estimated to undergo EHC 4.8 times per day in females and 4.1 times per day in males. Besides pool sizes, BA composition could be simulated even on suborgan level. Composition was exemplarily assessed in liver, portal blood, and skin in female mice (Figures 7B and S10). Model simulations showed that CA predominated in the liver, whereas in other organs MCAs constituted the most abundant BAs. The model was further used to simulate BA pools along the EHC and the gut axis (Figures 7C and S11). The model suggested a relative accumulation within the liver and the intestinal lumen, similar to other rodents where 70%–95% of BAs are found in the lumen.[41,42] Along the gut axis,

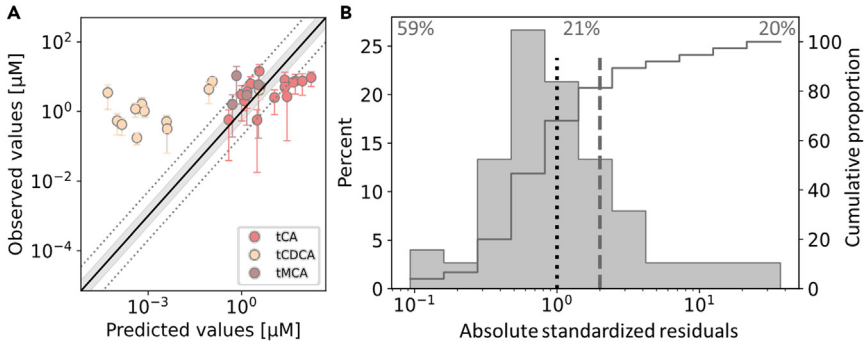


**Figure 5. Model prediction of germ-free mice**

Model predictions of concentration of bile acids in both male and female, germ-free mice against corresponding data points used for fitting.

(A) Only data points with a coefficient of variation below 1 are shown. Unity is indicated as a solid black line and a 2- and 5-fold range between predicted and observed values is indicated as a gray area or with dotted lines, respectively. Error bars represent the standard deviation.

(B) Distribution of the absolute standardized residual model predictions (histogram) and the corresponding cumulative function (line). The dotted and dashed lines indicate differences between model simulation and measured data of one SD and two SDs, respectively. Cumulative proportions of predictions that are within one SD (top left, residuals left of dotted line), between one and two SDs (top middle, residuals between dotted and dashed line), and above two SDs (top right, residuals right of dashed line) of measured data are stated at the top of the panel. See also Figure S8.

bile acids accumulated strongly in the cecum and thus gave rise to higher levels throughout the LI. This coincides with the reduced transporter expression (Figure 3A) as well as intestinal transit rate (data not shown) in the cecum compared with the ileum.

Apart from functional analyses of bile acid metabolism, the model could also be used to simulate physiological scenarios that had not been considered for model development. We here investigated in particular the functional effect of pathophysiological alterations on BA metabolism. To this end, the effect of bile acid malabsorption (BAM) as well as impaired intestinal barrier function on BA levels were simulated (Figures 8 and S12). For BAM, impaired reabsorption in the terminal ileum (Figure 8A) as well as increased BA synthesis (Figure 8B) were considered.[43] Defective BA uptake by the ileal mucosa showed overall minor effects on BA pool sizes. Only within the LI, both tissue and lumen, increasing BA amounts could be observed. Increasing BA synthesis resulted in overall elevated BA levels, with the strongest effect on the LI and SI lumen and liver. Disruption of the intestinal barrier function depleted BA pools within the gut lumen, whereas in liver as well as venous and portal blood plasma, BAs accumulated by 14- and 10-fold, respectively (Figure 8C). Although the same trend was present in male mice, the accumulation of BAs was not as pronounced as in female mice, showing a 4- and 3-fold difference, respectively (Figure S12F).

## DISCUSSION

In this work, we established a physiologically based model of bile acid metabolism in mice. The model describes the systemic circulation, synthesis, hepatic and microbial conversions, and excretion of the most abundant BAs. It further addresses sex differences in BA concentration and composition that have been reported in the literature before but that were also prominent in our experimental dataset. The model was carefully established and validated with an extensive dataset specifically sampled from both male and female SPF mice. Thus, the model integrates and contextualizes heterogeneous data including BA concentration in different organs, transporter expression along the gut segments, physiological parameters, and microbial composition in the cecum. Of particular note, the model suggested upregulation of BA synthesis and the transporter NTCP in female SPF mice. This observation, which is in agreement to earlier findings,[36,37] is an independent outcome of the model development process and had not been considered as prior knowledge for model building.

Furthermore, the resulting model for SPF mice could be used to predict BA measurements in GF mice by specifically eliminating microbial processes. This, along with the performed sensitivity analysis, is a strong indication for the overall model quality and provides confidence that the model can be used for further analyses and predictions. The model was next extended with additional information specifying physiological parameters and intestinal transporter expression in GF mice. We found that upregulation of BA synthesis, as reported in literature,[38–40] was not sufficient to explain BA levels in GF mice but had to be complemented by additional expressional changes in the liver. Unrestricted model predictions suggested that BA synthesis might be downregulated. It remains to be investigated whether this discrepancy could be attributed to model inaccuracies or strain differences. This illustrates that the model can be applied for both extrapolation to unknown scenarios as well as contextualization of existing knowledge in a systemic manner, e.g., extrapolation to disease contexts or cross-species extrapolation.

Alterations in BA composition and dynamics have been associated with a plethora of diseases. Compositional changes have been reported for inflammatory bowel disease (IBD), ulcerative colitis, Crohn disease, liver cirrhosis, liver cancer, irritable bowel syndrome, short bowel syndrome, and obesity.[2,9,10] Impairments within the EHC of BA have been linked to cholestatic drug-induced liver injury, chronic liver disease, cholesterol gallstone disease, malabsorption, dyslipidemia, and atherosclerosis.[11–16] In this context, the model was applied to predict the effect of BA malabsorption (BAM) as cause for idiopathic BA diarrhea (BAD)[43] and impairment of the intestinal barrier function—as

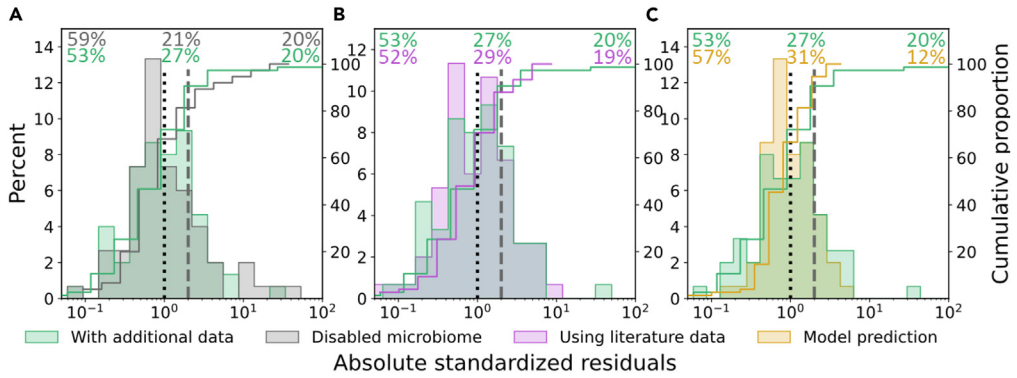


**Figure 6. Model prediction of changes in germ-free mice**

Comparison of different model variants for describing BA metabolism in germ-free mice by comparing the distribution of the absolute standardized residuals (histograms) and their corresponding cumulative function (lines). The dotted and dashed lines indicate differences between model simulation and measured data of one SD and two SDs, respectively. Cumulative proportions of predictions that lie within one SD (residuals left of dotted line), between one and two SDs (residuals between dotted and dashed line), and above two SDs (residuals right of dashed line) of measured data are stated at the top of the panel.

(A–C) A model variant with additional information about physiology and intestinal transporter expression (green) is compared with a simple extrapolation of the base model by disabling any microbial reaction (gray). The model variant with the additional information was also tested against model variants that introduce further expressional changes in the liver (B) according to literature (pink) or (C) as suggested by the model (yellow).

observed in celiac disease,[44–47] IBD,[48,49] and metabolic associated fatty liver disease (MAFLD)[50–52]—on BA metabolism. Consistent with other studies, our model showed that an increase in BA synthesis[14,53,54] and overflow of reabsorption resulted in a strong accumulation of BAs in the LI lumen, whereas malabsorption in the terminal ileum without ileal or other obvious gastrointestinal (GI) disease did not suffice to induce BAD.[55] As a first assessment of a "leaky gut," the paracellular intestinal permeability was altered in all gut segments equally. Further analyses may include other routes of transepithelial transport, i.e., transcellular or transporter-mediated, as well as regional differences in permeability as demonstrated by Thomson et al.[56] These predictions are possible because the model contains a detailed model of the GI tract.[57,58] As demonstrated, the model can shed light on the complex interaction between pathophysiological alteration, such as physiological or expressional changes, microbial dysbiosis but also drug administration, and bile acid metabolism. Future extensions of the model may include the consideration of food effects on gall bladder emptying as well as postprandial effects on bile acid plasma levels.

Investigating the link between BA metabolism and their role in human disease, various animal models have been applied, including lamprey, skate, zebrafish, rat, mouse, hamster, rabbit, prairie dog, and monkey.[59–61] Of the small animal models, hamsters are most similar to humans regarding BA metabolism[62–64]; nevertheless, mice remain the most commonly utilized animal model to investigate human metabolism.[17,18] Indicative of the difference between human and mice is the different bile acid composition.[6,19] The murine BA pool is heavily influenced by MCAs, increasing its hydrophilicity, lowering its cytotoxicity, and shifting to a more antagonistic FXR-signaling regime.[19] Further differences relevant for BA metabolism can be found in the physiology of the GI tract,[65–69] energy homeostasis,[70] and the recycling of nutrients and bile acids through coprophagy.[71,71] Therefore, extrapolation from mouse studies to humans for BA signaling or BA-related diseases are difficult. Addressing these concerns, a recent study used mouse models with a more human-like bile acid composition.[72] These "humanized" mice have single or double knockout in *Cyp2a12* and *Cyp2c70*, resulting in much more hydrophobic BA pools.[73,74] Initial model predictions for *Cyp2a12* knockout mice showed a strong accumulation of DCA, for *Cyp2c70* an absence of MCAs and increase in hepatobiliary CDCA, and for mice with double knockouts DCA, CDCA, and LCA were strongly increased (data not shown). These initial findings are overall in good agreement with reported BA composition in these mice.[74] This demonstrated that the computational model developed in this work might support cross-species extrapolation due to the mechanistic structure of the underlying PBPK model.[21]

Lastly, the model can assist in optimizing experimental designs for mouse studies that aim to elucidate the complex behavior of BAs in health and disease. This is especially relevant in the context of the "3R" principles proposed by Russel and Burch in 1959[75]: Reduction, Refinement, and Replacement of animal testing. In this context, we demonstrated that the model can predict BA level and composition throughout the body, most notably in experimentally not easily accessible organs, e.g., the liver or portal blood, under both physiological and pathophysiological conditions. Based on the same model predictions, the BA pool was estimated to be recycled four to five times per day in contrast to four to twelve times in humans.[76] This represents a first assessment of species differences between mouse and human. All of these predictions could be made without further animal sacrifice. We believe that the here presented model can serve as a useful platform for model-aided investigation of BA metabolism in prospective studies.

## Limitation of the study

Future analysis with the physiologically based model may introduce structural mechanistic revisions. In this version of the computational model, we included only the most abundant bile acid species but disregarded conjugation, sulfation, and distinction of $\alpha/\beta/\omega$-MCA. Our model can therefore not capture the full complexity of the BA pool and might introduce a systemic bias in our predictions as different BA species do

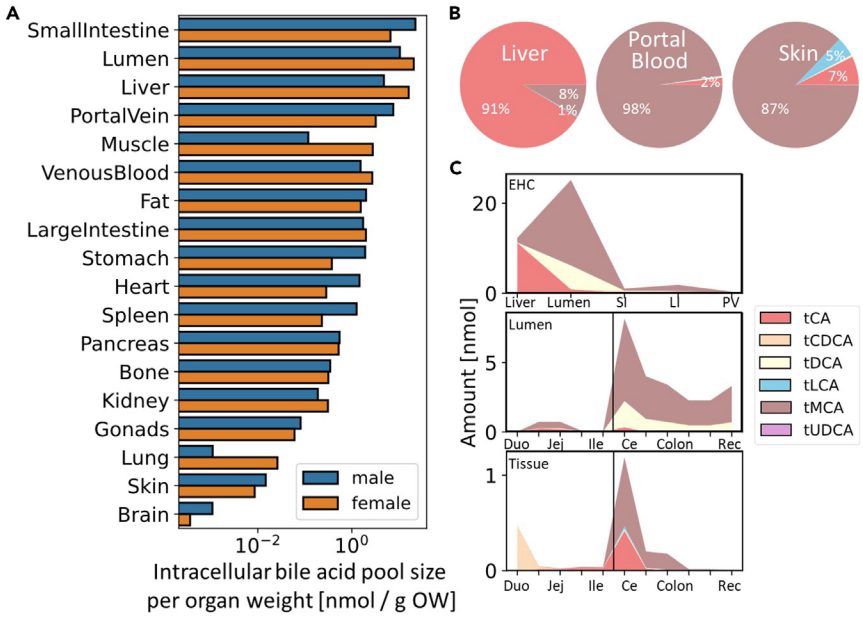


**Figure 7. Model-based BA pool distribution and composition at the whole-body level**

(A–C) Simulated bile acid pool sizes per organ weight in different organs in male and female mice (A) and model-based bile acid composition in liver, portal blood plasma, and skin in female mice (B) as well as simulated bile acid pools along the EHC and gut axis (C). For the EHC axis, BA level and composition are shown in liver, the intestinal lumen, small and large intestinal tissue (SI and LI), as well as portal blood plasma (PV). Along the gut axis, duodenum (Duo), jejunum (Jej), ileum (Ile), cecum (Ce), proximal and distal colon (Colon), and rectum (Rec) are shown, and the transition of SI and LI are indicated by a vertical black line. See also Figures S9–S11.

not have the same kinetics.[77] Furthermore, we had to simplify the dynamic behavior of BA circulation. In the computational model, all BAs are secreted directly into the duodenum omitting the gallbladder. Thus, postprandial responses but also coprophagy, as a means of BA recycling,[71,78] were neglected as these effects are difficult to describe mechanistically in mice. Consequently, the model cannot capture effects of the circadian rhythm as observed in other rodents.[41,42,79,80] Omitting the gallbladder, our model does not account for a considerable BA pool. Assuming a gallbladder volume of a few µl[81,82] and BA concentration in bile measured here, we estimate the BA pool size in gallbladder to be in the lower nmol range. We further simplified the model by only considering expression of the main BA transporters and enzymes involved in BA synthesis in the main organs of the EHC. Inclusion of expression levels of BA transporters and enzymes, which were neglected here, might especially benefit and improve predictions of BA levels in non-EHC organs. In this context, expression of OATPs, MRP2, and OST $\alpha/\beta$ in liver and of CYP27A1 and CYP7B1 in nonhepatic tissues might be especially interesting. Moreover, the microbiota was only assessed in the cecum. The murine cecum is quite large and functions as a microbial fermentation vessel[65]; however, variation in the microbial composition in other gut segments might contribute to the observed sex differences. Previous studies have also shown that similar microbial communities might be enriched

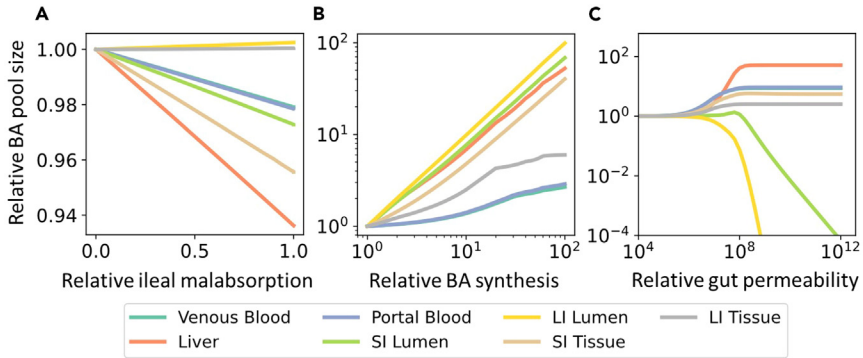


**Figure 8. Model prediction of BA pool sizes in BA malabsorption and loss of intestinal barrier function**

(A–C) Predicted changes in bile acid pool sizes in different organs in female mice for decreasing BA absorption in the terminal ileum (A), increasing BA synthesis (B), as well as increasing paracellular permeability along the whole gut (C). See also Figure S12.

for different functions.[83] Besides compositional variation, there might be differences in microbial density between male and female mice, which have not been assessed in this study. Despite these limitations, the model was able to recapitulate BA composition and levels at the whole-body level and account for sex-related differences in BA metabolism, both with good accuracy.

## STAR★METHODS

Detailed methods are provided in the online version of this paper and include the following:

- KEY RESOURCES TABLE
- RESOURCE AVAILABILITY
  - Lead contact
  - Materials availability
  - Data and code availability
- EXPERIMENTAL MODEL AND STUDY PARTICIPANT DETAILS
  - Mouse housing conditions and sampling
- METHOD DETAILS
  - Bile acid measurements
  - Microbiota analysis by high-throughput sequencing
  - Computational methods
- QUANTIFICATION AND STATISTICAL ANALYSIS

## SUPPLEMENTAL INFORMATION

Supplemental information can be found online at https://doi.org/10.1016/j.isci.2023.107922.

## ACKNOWLEDGMENTS

We thank Vanessa Baier and Zita Soons for the helpful discussions. We are grateful to Ntana Kousetzi (Functional Microbiome Research Group, Institute of Medical Microbiology, RWTH University Hospital) for outstanding technical support with microbiota analysis by sequencing. This manuscript has been released as a Pre-Print at bioRxiv.[84] Funding was provided from the German Research Foundation (DFG)—Project-ID 403224013—"SFB 1382". MvB is thankful for support by Novo Nordisk Foundation grant NNF21OC0066551. MvB and URK are grateful for funding of the UFZ for the ProMetheus platform for proteomics and metabolomics.

## AUTHOR CONTRIBUTIONS

Bastian Kister: Methodology, Software, Validation, Formal analysis, Writing—original draft, Writing—review & editing, Visualization. Alina Viehof: Methodology, Investigation, Writing—review & editing. Ulrike Rolle-Kampczyk: Investigation, Writing—review & editing. Annika Schwentker: Investigation Nicole Simone Treichel: Formal analysis, Investigation, Writing–review & editing. Susan Jennings: Investigation. Theresa H. Wirtz: Writing—review & editing. Lars M. Blank: Writing—review & editing. Mathias W. Hornef: Resources, Writing—review & editing. Martin von Bergen: Resources, Writing—review & editing. Thomas Clavel: Resources, Writing—review & editing. Lars Kuepfer: Conceptualization, Resources, Writing—original draft, Writing—review & editing, Supervision.

## DECLARATION OF INTERESTS

The authors have no conflicts of interest to declare.

Received: February 16, 2023
Revised: July 4, 2023
Accepted: September 12, 2023
Published: September 17, 2023

## REFERENCES

1. Schaap, F.G., Trauner, M., and Jansen, P.L.M. (2014). Bile acid receptors as targets for drug development. Nat. Rev. Gastroenterol. Hepatol. *11.1*, 55–67. https://doi.org/10.1038/nrgastro.2013.151.
2. Wahlström, A., Sayin S.I., Marschall H.U., Bäckhed F. (2016). Intestinal Crosstalk between Bile Acids and Microbiota and Its Impact on Host Metabolism. Cell Metabol. *24.1*, 41–50. https://doi.org/10.1016/j.cmet.2016.05.005. http://www.sciencedirect.com/science/article/pii/S1550413116302236.
3. J.M. Ridlon, Harris, S.C., Bhowmik, S., Kang, D.J., Hylemon, P.B.. Consequences of bile salt biotransformations by intestinal bacteria". In: Gut Microb. 7.22–39. https://doi.org/10.1080/19490976.2015.1127483.
4. Russell, D.W. (2003). The Enzymes, Regulation, and Genetics of Bile Acid Synthesis. Annu. Rev. Biochem. *72.1*, 137–174. https://doi.org/10.1146/annurev.biochem.72.121801.161712.
5. Jason, M. (2006). Ridlon, Dae-Joong Kang, and Phillip B. Hylemon. "Bile salt biotransformations by human intestinal bacteria". J. Lipid Res. *47.2*, 241–259. https://doi.org/10.1194/jlr.R500013-JLR200.
6. Li, J., Paul, A., and Dawson. (2019). Animal models to study bile acid metabolism. Biochim Biophys Acta Mol Basis Dis, 895–911. https://doi.org/10.1016/j.bbadis.2018.05.

011. http://www.sciencedirect.com/science/article/pii/S0925443918301819.
7. S. Marion, Studer, N., Desharnais, L., Menin, L., Escrig, S., Meibom, A., Hapfelmeier, S., Bernier-Latmani, R..In vitro and in vivo characterization of Clostridium scindens bile acid transformations". In: Gut Microb. 10.481–503. https://doi.org/10.1080/19490976.2018.1549420.
8. Eyssen, H., De Pauw, G., Stragier, J., and Verhulst, A. (1983). Cooperative formation of omega-muricholic acid by intestinal microorganisms. Appl. Environ. Microbiol. *45.1*, 141–147. https://doi.org/10.1128/aem.45.1.141-147.1983.
9. C. Staley, Weingarden, A.R., Khoruts, A., Sadowsky, M.J.. Interaction of gut microbiota with bile acid metabolism and its influence on disease states". Appl. Microbiol. Biotechnol. 101.47–64. ISSN: 0175-7598. https://www.ncbi.nlm.nih.gov/pmc/articles/PMC5203956/.
10. Duboc, H., Rajca, S., Rainteau, D., Benarous, D., Maubert, M.A., Quervain, E., Thomas, G., Barbu, V., Humbert, L., Despras, G., et al. (2013). Connecting dysbiosis, bile-acid dysmetabolismand gut inflammation in inflammatory bowel diseases. Gut *62.4*, 531–539. https://doi.org/10.1136/gutjnl-2012-302578. https://gut.bmj.com/content/62/4/531.full.pdf.
11. Wagner, M., and Trauner, M. (2016). Recent advances in understanding and managing cholestasis [version 1; peer review: 2 approved. F1000Res. *5*, 705. https://doi.org/10.12688/f1000research.8012.1.
12. Jackson, J.P., Freeman, K.M., Friley, W.W., St. Claire, R.L., Black, C., and Brouwer, K.R. (2016). Basolateral Efflux Transporters: A Potentially Important Pathway for the Prevention of Cholestatic Hepatotoxicity. Appl. In Vitro Toxicol. *2.4*, 207–216. https://doi.org/10.1089/aivt.2016.0023.
13. Eduardo Rui Castro and Maria Pereira Cecília Rodrigues (2017). Cell Death and microRNAs in Cholestatic Liver Diseases: Update on Potential Therapeutic Applications. https://doi.org/10.2174/1389450116666151019102358. http://www.eurekaselect.com/article/71155.
14. Walters, J.R.F., Tasleem, A.M., Omer, O.S., Brydon, W.G., Dew, T., and le Roux, C.W. (2009). A New Mechanism for Bile Acid Diarrhea: Defective Feedback Inhibition of Bile Acid Biosynthesis. Clin. Gastroenterol. Hepatol. *7.11*, 1189–1194. https://doi.org/10.1016/j.cgh.2009.04.024. https://www.sciencedirect.com/science/article/pii/S1542356509004339.
15. Degen, L.P., and Phillips, S.F. (1996). Variability of gastrointestinal transit in healthy women and men. Gut *39.2*, 299–305. https://doi.org/10.1136/gut.39.2.299. https://gut.bmj.com/content/39/2/299.full.pdf.
16. Guicciardi, M.E., and Gores, G.J. (2002). Bile acid-mediated hepatocyte apoptosis and cholestatic liver disease. Dig. Liver Dis. *34.6*, 387–392. https://doi.org/10.1016/S1590-8658(02)80033-0. https://www.sciencedirect.com/science/article/pii/S1590865802800330.
17. Rosenthal, N., and Brown, S. (2007). The mouse ascending: perspectives for human-disease models. Nat. Cell Biol. *9.9*, 993–999. https://doi.org/10.1038/ncb437.
18. Janan, T. (2017). Eppig. "Mouse Genome Informatics (MGI) Resource: Genetic, Genomic, and Biological Knowledgebase for the Laboratory Mouse". ILAR J. *58.1*, 17–41. https://doi.org/10.1093/ilar/ilx013. https://academic.oup.com/ilarjournal/articlepdf/58/1/17/24325222/ilx013.pdf.
19. Thakare, R., Alamoudi, J.A., Gautam, N., Rodrigues, A.D., and Alnouti, Y. (2018). Species differences in bile acids I. Plasma and urine bile acid composition. J. Appl. Toxicol. *38.10*, 1323–1335. https://doi.org/10.1002/jat.3644.
20. Kuepfer, L., Niederalt, C., Wendl, T., Schlender, J., Willmann, S., Lippert, J., Block, M., Eissing, T., and Teutonico, D. (2016). Applied Concepts in PBPK Modeling: How to Build a PBPK/PD Model. CPT Pharmacometrics Syst. Pharmacol. *5.10*, 516–531. https://doi.org/10.1002/psp4.12134.
21. Thiel, C., Schneckener, S., Krauss, M., Ghallab, A., Hofmann, U., Kanacher, T., Zellmer, S., Gebhardt, R., Hengstler, J.G., and Kuepfer, L. (2015). A systematic evaluation of the use of physiologically based pharmacokinetic modeling for cross-species extrapolation. J. Pharmaceut. Sci. *104*, 191–206.
22. Schenk, A., Ghallab, A., Hofmann, U., Hassan, R., Schwarz, M., Schuppert, A., Schwen, L.O., Braeuning, A., Teutonico, D., Hengstler, J.G., and Kuepfer, L. (2017). Physiologically-based modelling in mice suggests an aggravated loss of clearance capacity after toxic liver damage. Sci. Rep. *7.1*, 6224. https://doi.org/10.1038/s41598-017-04574-z.
23. Krauss, M., Schaller, S., Borchers, S., Findeisen, R., Lippert, J., and Kuepfer, L. (2012). Integrating Cellular Metabolism into a Multiscale Whole-Body Model. PLoS Comput. Biol. *8*, 1–13. https://doi.org/10.1371/journal.pcbi.1002750.
24. Wahlström, A., Al-Dury, S., Ståhlman, M., Bäckhed, F., and Marschall, H.U. (2017). Cyp3a11 is not essential for the formation of murine bile acids. Biochem. Biophys. Rep. *10*, 70–75. https://doi.org/10.1016/j.bbrep.2017.02.011. http://www.sciencedirect.com/science/article/pii/S240558081730002X.
25. Chen, J., Bittinger, K., Charlson, E.S., Hoffmann, C., Lewis, J., Wu, G.D., Collman, R.G., Bushman, F.D., and Li, H. (2012). Associating microbiome composition with environmental covariates using generalized UniFrac distances. *Bioinformatics* (Oxford, England) *28*, 2106–2113.
26. Lozupone, C., and Knight, R. (2005). "UniFrac: a new phylogenetic method for comparing microbial communities". Appl. Environ. Microbiol. *71*, 8228–8235.
27. O'Flaherty, S., Briner Crawley A., Theriot C.M., Barrangou R. (2018). "The Lactobacillus Bile Salt Hydrolase Repertoire Reveals Niche-Specific Adaptation". mSphere *3*.
28. Wishart, D.S., Guo, A., Oler, E., Wang, F., Anjum, A., Peters, H., Dizon, R., Sayeeda, Z., Tian, S., Lee, B.L., et al. (2022). HMDB 5.0: the Human Metabolome Database for 2022. Nucleic Acids Res. *50*, D622–D631. https://doi.org/10.1093/nar/gkab1062. eprint. https://academic.oup.com/nar/articlepdf/50/D1/D622/42058215/gkab1062.pdf.
29. Heuman, D.M., Hylemon, P.B., and Vlahcevic, Z.R. (1989). Regulation of bile acid synthesis. III. Correlation between biliary bile salt hydrophobicity index and the activities of enzymes regulating cholesterol and bile acid synthesis in the rat. J. Lipid Res. *30*, 1161–1171.
30. Watanabe, M., Horai Y., Houten S.M., Morimoto K., Sugizaki T., Arita E., Mataki C., Sato H., Tanigawara Y., Schoonjans K., et al. (2011). Lowering bile acid pool size with a synthetic farnesoid X receptor (FXR) agonist induces obesity and diabetes through reduced energy expenditure". eng. J. Biol. Chem. *286*, 26913–26920. https://www.ncbi.nlm.nih.gov/pmc/articles/PMC3143650/.
31. Jung, D., Inagaki T., Gerard R.D., Dawson P.A., Kliewer S.A., Mangelsdorf D.J., Moschetta A. (2007). "FXR agonists and FGF15 reduce fecal bile acid excretion in a mouse model of bile acid malabsorption". eng. J. Lipid Res. *48*, 2693–2700. https://www.ncbi.nlm.nih.gov/pubmed/17823457.
32. L. Yu, Li-Hawkins, J., Hammer, R.E., Berge, K.E., Horton, J.D., Cohen, J.C., Hobbs, H.H.. Overexpression of ABCG5 and ABCG8 promotes biliary cholesterol secretion and reduces fractional absorption of dietary cholesterol". In: J. Clin. Invest. 110.671–680. https://doi.org/10.1172/JCI16001.
33. Dawson, P.A., Haywood J., Craddock A.L., Wilson M., Tietjen M., Kluckman K., Maeda N., Parks J.S. (2003). "Targeted deletion of the ileal bile acid transporter eliminates enterohepatic cycling of bile acids in mice". eng. J. Biol. Chem. *278*, 33920–33927. https://www.ncbi.nlm.nih.gov/pubmed/12819193.
34. Marschall, H.-U., Wagner M., Bodin K., Zollner G., Fickert P., Gumhold J., Silbert D., Fuchsbichler A., Sjoevall J. Trauner M. (2006). Fxr(-/-) mice adapt to biliary obstruction by enhanced phase I detoxification and renal elimination of bile acids". eng. J. Lipid Res. *47*, 582–592. https://pubmed.ncbi.nlm.nih.gov/16327028.
35. Tannock, G.W., Dashkevicz, M.P., and Feighner, S.D. (1989). "Lactobacilli and bile salt hydrolase in the murine intestinal tract. Appl. Environ. Microbiol. *55.7*, 1848–1851. https://aem.asm.org/content/55/7/1848.full.pdf.
36. Link, J.C., Chen, X., Prien, C., Borja, M.S., Hammerson, B., Oda, M.N., Arnold, A.P., and Reue, K. (2015). Increased High-Density Lipoprotein Cholesterol Levels in Mice With XX Versus XY Sex Chromosomes. Arterioscler. Thromb. Vasc. Biol. *35.8*, 1778–1786. https://doi.org/10.1161/atvbaha.115.305460.
37. Cheng, X., Buckley, D., and Klaassen, C.D. (2007). Regulation of hepatic bile acid transporters Ntcp and Bsep expression. Biochem. Pharmacol. *74*, 1665–1676.
38. Wahlström, A., Kovatcheva-Datchary, P., Ståhlman, M., Khan, M.T., Bäckhed, F., and Marschall, H.U. (2017). Induction of farnesoid X receptor signaling in germ-free mice colonized with a human microbiota. J. Lipid Res. *58*, 412–419.
39. Sayin, S.I., Wahlström, A., Felin, J., Jäntti, S., Marschall, H.U., Bamberg, K., Angelin, B., Hyötyläinen, T., Orešič, M., and Bäckhed, F. (2013). Gut Microbiota Regulates Bile Acid Metabolism by Reducing the Levels of Tauro-beta-muricholic Acid, a Naturally Occurring FXR Antagonist. Cell Metabol. *17.2*, 225–235. https://doi.org/10.1016/j.cmet.2013.01.003. http://www.sciencedirect.com/science/article/pii/S1550413113000119.
40. Li, F., Jiang, C., Krausz, K.W., Li, Y., Albert, I., Hao, H., Fabre, K.M., Mitchell, J.B., Patterson, A.D., and Gonzalez, F.J. (2013). Microbiome remodelling leads to inhibition of intestinal farnesoid X receptor signalling and decreased obesity. Nat. Commun. *4*, 2384.
41. Ho, K.J. (1976). Circadian distribution of bile acid in the enterohepatic circulatory system in hamsters. J. Lipid Res. *17*, 600–604.

42. Ho, K.J. (1976). Circadian distribution of bile acids in the enterohepatic circulatory system in rats. Am. J. Phys. *230*, 1331–1335.
43. Camilleri, M. (2015). Bile Acid diarrhea: prevalence, pathogenesis, and therapy. Gut Liver *9*, 332–339.
44. Smecuol, E., Bai, J.C., Vazquez, H., Kogan, Z., Cabanne, A., Niveloni, S., Pedreira, S., Boerr, L., Mauriño, E., and Meddings, J.B. (1997). Gastrointestinal permeability in celiac disease. Gastroenterology *112.4*, 1129–1136. https://doi.org/10.1016/S0016-5085(97)70123-9. https://www.sciencedirect.com/science/article/pii/S0016508597701239.
45. Bjarnason, I., Peters, T.J., and Veall, N. (1983). A PERSISTENT DEFECT IN INTESTINAL PERMEABILITY IN COELIAC DISEASE DEMONSTRATED BY A 51Cr-LABELLED EDTA ABSORPTION TEST. Lancet *321*, 323–325. https://doi.org/10.1016/S0140-6736(83)91628-8. https://www.sciencedirect.com/science/article/pii/S0140673683916288.
46. Schulzke, J.D., Schulzke, I., Fromm, M., and Riecken, E.O. (1995). Epithelial barrier and ion transport in coeliac sprue: electrical measurements on intestinal aspiration biopsy specimens. Gut *37.6*, 777–782. https://doi.org/10.1136/gut.37.6.777.
47. Schumann, M., Günzel, D., Buergel, N., Richter, J.F., Troeger, H., May, C., Fromm, A., Sorgenfrei, D., Daum, S., Bojarski, C., et al. (2012). Cell polarity-determining proteins Par-3 and PP-1 are involved in epithelial tight junction defects in coeliac disease. Gut *61.2*, 220–228. https://doi.org/10.1136/gutjnl-2011-300123.
48. Casellas, F., Aguade, S., Soriano, B., Accarino, A., Molero, J., and Guarner, L. (1986). Intestinal Permeability to 99m Tc–Diethylenetriaminopentaacetic Acid in Inflammatory Bowel Disease. Am. J. Gastroenterol. *81*, 767–770.
49. Jenkins R.T., Ramage J.K., Jones D.B., Collins S.M., Goodacre R.L., Hunt R.H.Small bowel and colonic permeability to 51Cr-EDTA in patients with active inflammatory bowel diseaseClin. Invest. Med.198811.2151155 http://europepmc.org/abstract/MED/3135136
50. Pierri L., Saggese P., Guercio Nuzio S., Troisi J., Di Stasi M., Poeta M., Savastano R., Marchese G., Tarallo R., Bergheim I.,et al. Relations of Gut Liver axis Components and Gut Microbiota in Obese Children with Fatty Liver: A Pilot Study. 2018.
51. Wigg, A.J., Roberts-Thomson, I.C., Dymock, R.B., McCarthy, P.J., Grose, R.H., and Cummins, A.G. (2001). The role of small intestinal bacterial overgrowth, intestinal permeability, endotoxaemia, and tumour necrosis factor α in the pathogenesis of non-alcoholic steatohepatitis. Gut *48*, 206–211. https://doi.org/10.1136/gut.48.2.206. https://gut.bmj.com/content/48/2/206.full.pdf.
52. Farhadi, A., Gundlapalli, S., Shaikh, M., Frantzides, C., Harrell, L., Kwasny, M.M., and Keshavarzian, A. (2008). Susceptibility to gut leakiness: a possible mechanism for endotoxaemia in non-alcoholic steatohepatitis. Liver Int. *28.7*, 1026–1033. https://doi.org/10.1111/j.1478-3231.2008.01723.x.
53. Rao, A.S., Wong, B.S., Camilleri, M., Odunsi-Shiyanbade, S.T., McKinzie, S., Ryks, M., Burton, D., Carlson, P., Lamsam, J., Sing, R., and Zinsmeister, A.R. (2010). Chenodeoxycholate in females with irritable bowel syndrome-constipation: a pharmacodynamic and pharmacogenetic analysis. Gastroenterology *139*, 1549–1558.
54. Wong, B.S., Camilleri, M., Carlson, P., McKinzie, S., Busciglio, I., Bondar, O., Dyer, R.B., Lamsam, J., and Zinsmeister, A.R. (2012). Increased bile acid biosynthesis is associated with irritable bowel syndrome with diarrhea. Clin. Gastroenterol. Hepatol. *10*, 1009–1015.e3.
55. Bajor, A., Kilander, A., Fae, A., G??lman, C., Jonsson, O., ??hman, L., Rudling, M., Sj??vall, H., Stotzer, P.O., and Ung, K.A. (2006). Normal or increased bile acid uptake in isolated mucosa from patients with bile acid malabsorption. Eur. J. Gastroenterol. Hepatol. *18*, 397–403. https://journals.lww.com/eurojgh/Fulltext/2006/04000/Normal_or_increased_bile_acid_uptake_in_isolated.13.aspx.
56. Thomson, A., Smart, K., Somerville, M.S., Lauder, S.N., Appanna, G., Horwood, J., Sunder Raj, L., Srivastava, B., Durai, D., Scurr, M.J., et al. (2019). The Ussing chamber system for measuring intestinal permeability in health and disease. BMC Gastroenterol. *19.1*, 98. https://doi.org/10.1186/s12876-019-1002-4.
57. Thelen, K., Coboeken, K., Willmann, S., Burghaus, R., Dressman, J.B., and Lippert, J. (2011). Evolution of a detailed physiological model to simulate the gastrointestinal transit and absorption process in humans, Part 1: Oral solutions. J. Pharmaceut. Sci. *100.12*, 5324–5345. https://doi.org/10.1002/jps.22726.
58. Thelen, K., Coboeken, K., Willmann, S., Dressman, J.B., and Lippert, J. (2012). Evolution of a detailed physiological model to simulate the gastrointestinal transit and absorption process in humans, part II: Extension to describe performance of solid dosage forms. J. Pharmaceut. Sci. *101.3*, 1267–1280. https://doi.org/10.1002/jps.22825.
59. Baghdasaryan, A., Fuchs, C.D., Oesterreicher, C.H., Lemberger, U.J., Halibasic, E., Pahlman, I., Graffner, H., Krones, E., Fickert, P., Wahlstroem, A., et al. (2016). Inhibition of intestinal bile acid absorption improves cholestatic liver and bile duct injury in a mouse model of sclerosing cholangitis. J. Hepatol. *64*, 674–681. https://doi.org/10.1016/j.jhep.2015.10.024. https://www.sciencedirect.com/science/article/pii/S0168827815007230.
60. Benjamin, L. (2012). Woolbright and Hartmut Jaeschke. "Novel insight into mechanisms of cholestatic liver injury. World J. Gastroenterol. *18*, 4985–4993.
61. Jansen, P.L.M., Ghallab, A., Vartak, N., Reif, R., Schaap, F.G., Hampe, J., and Hengstler, J.G. (2017). The ascending pathophysiology of cholestatic liver disease. Hepatology *65*, 722–738. https://doi.org/10.1002/hep.28965.
62. Dietschy, J.M., Turley, S.D., and Spady, D.K. (1993). Role of liver in the maintenance of cholesterol and low density lipoprotein homeostasis in different animal species, including humans. J. Lipid Res. *34.10*, 1637–1659. https://doi.org/10.1016/S0022-2275(20)35728-X. https://www.sciencedirect.com/science/article/pii/S002222752035728X.
63. Gurantz, D., and Hofmann, A.F. (1984). Influence of bile acid structure on bile flow and biliary lipid secretion in the hamster. Am. J. Physiol. Gastrointest. Liver Physiol. *247*, G736–G748. https://doi.org/10.1152/ajpgi.1984.247.6.G736.
64. van Golen, R.F., Olthof, P.B., de Haan, L.R., Coelen, R.J., Pechlivanis, A., de Keijzer, M.J., Weijer, R., de Waart, D.R., van Kuilenburg, A.B.P., Roelofsen, J., et al. (2018). The pathophysiology of human obstructive cholestasis is mimicked in cholestatic Gold Syrian hamsters. Biochim. Biophys. Acta, Mol. Basis Dis. *1864*, 942–951. https://doi.org/10.1016/j.bbadis.2017.11.022. https://www.sciencedirect.com/science/article/pii/S0925443917304441.
65. Hugenholtz, F., Willem, M., and de Vos. (2018). "Mouse models for human intestinal microbiota research: a critical evaluation". Cell. Mol. Life Sci. *75*, 149–160. https://doi.org/10.1007/s00018-017-2693-8. https://www.ncbi.nlm.nih.gov/pmc/articles/PMC5752736/.
66. Ghoshal, N.G., and Bal, H.S. (1989). Comparative morphology of the stomach of some laboratory mammals. Lab. Animals *23*, 21–29.
67. McConnell, E.L., Basit, A.W., and Murdan, S. (2008). Measurements of rat and mouse gastrointestinal pH, fluid and lymphoid tissue, and implications for in-vivo experiments. J. Pharm. Pharmacol. *60*, 63–70.
68. Booijink, C.C., Zoetendal, E.G., Kleerebezem, M., and de Vos, W.M. (2007). Microbial communities in the human small intestine: coupling diversity to metagenomics. Future Microbiol. *2*, 285–295.
69. Sheridan, W.G., Lowndes, R.H., and Young, H.L. (1990). "Intraoperative tissue oximetry in the human gastrointestinal tract." eng. Am. J. Surg. *159*, 314–319.
70. Kleiber, M. (1975). Metabolic turnover rate: a physiological meaning of the metabolic rate per unit body weight. J. Theor. Biol. *53*, 199–204.
71. Sakaguchi, E. (2003). Digestive strategies of small hindgut fermenters. Anim. Sci. J. *74.5*, 327–337. https://doi.org/10.1046/j.1344-3941.2003.00124.x.
72. Ueda, H., Honda, A., Miyazaki, T., Morishita, Y., Hirayama, T., Iwamoto, J., Nakamoto, N., and Ikegami, T. (2022). Sex-age-and organ-dependent improvement of bile acid hydrophobicity by ursodeoxycholic acid treatment: A study using a mouse model with human-like bile acid composition. PLoS One *17.7*, e0271308–e0271318. https://doi.org/10.1371/journal.pone.0271308.
73. de Boer, J.F., Verkade, E., Mulder, N.L., de Vries, H.D., Huijkman, N., Koehorst, M., Boer, T., Wolters, J.C., Bloks, V.W., van de Sluis, B., and Kuipers, F. (. 2020). A human-like bile acid pool induced by deletion of hepatic *Cyp2c70* modulates effects of FXR activation in mice [S]. J. Lipid Res. *61.3*, 291–305. https://doi.org/10.1194/jlr.RA119000243.
74. Honda, A., Miyazaki, T., Iwamoto, J., Hirayama, T., Morishita, Y., Monma, T., Ueda, H., Mizuno, S., Sugiyama, F., Takahashi, S., and Ikegami, T. (2020). Regulation of bile acid metabolism in mouse models with hydrophobic bile acid composition." eng. J. Lipid Res. *61*, 54–69.
75. William Moy Stratton Russell and Rex Leonard Burch (1959). The Principles of Humane Experimental Technique (Methuen).
76. Mok, H.Y.I., von Bergmann, K., and Grundy, S.M. (1977). Regulation of Pool Size of Bile Acids in Man. Gastroenterology *73.4*, 684–690. https://doi.org/10.1016/S0016-5085(19)31766-4. https://www.sciencedirect.com/science/article/pii/S0016508519317664.
77. Setchell, K.D., Rodrigues, C.M., Clerici, C., Solinas, A., Morelli, A., Gartung, C., and

Boyer, J. (1997). Bile acid concentrations in human and rat liver tissue and in hepatocyte nuclei. Gastroenterology *112*, 226–235.

78. Klaasen, H.L.B.M., Koopman, J.P., Scholten, P.M., Van Den Brink, M.E., and Theeuwes, A.G.M. (1990). Effect of Preventing Coprophagy on Colonisation by Segmented Filamentous Bacteria in the Small Bowel of Mice. Microb. Ecol. Health Dis. *3.2*, 99–103. https://doi.org/10.3109/08910609009140123.
79. Zhang, Y.-K.J., Guo, G.L., and Klaassen, C.D. (2011). Diurnal variations of mouse plasma and hepatic bile acid concentrations as well as expression of biosynthetic enzymes andb transporters. PLoS One *6*, e16683.
80. H.M. Eggink, Oosterman, J.E., de Goede, P., de Vries, E.M., Foppen, E., Koehorst, M., Groen, A.K., Boelen, A., Romijn, J.A., la Fleur, S.E., et al., . Complex interaction between circadian rhythm and diet on bile acid homeostasis in male rats". In: Chronobiol. Int. 34.1339–1353. https://doi.org/10.1080/07420528.2017.1363226.
81. Cheng, K., Metry, M., Felton, J., Shang, A.C., Drachenberg, C.B., Xu, S., Zhan, M., Schumacher, J., Guo, G.L., Polli, J.E., and Raufman, J.P. (2018). Diminished gallbladder filling, increased fecal bile acids, and promotion of colon epithelial cell proliferation and neoplasia in fibroblast growth factor 15-deficient mice. Oncotarget *9.39*, 25572–25585. https://doi.org/10.18632/oncotarget.25385.
82. van Erpecum, K.J., Wang, D.Q.H., Moschetta, A., Ferri, D., Svelto, M., Portincasa, P., Hendrickx, J.J., Schipper, M., and Calamita, G. (2006). Gallbladder histopathology during murine gallstone formation: relation to motility and concentrating function. J. Lipid Res. *47*, 32–41. https://doi.org/10.1194/jlr.M500180-JLR200. https://www.sciencedirect.com/science/article/pii/S002222752033652X.
83. Yilmaz, B., Juillerat, P., Øyås, O., Ramon, C., Bravo, F.D., Franc, Y., Fournier, N., Michetti, P., Mueller, C., Geuking, M., et al. (2019). Microbial network disturbances in relapsing refractory Crohn's disease. Nat. Med. *25.2*, 323–336. https://doi.org/10.1038/s41591-018-0308-z.
84. Kister, B., Viehof, A., Rolle-Kampczyk, U., Schwentker, A., Treichel, N.S., Jennings, S., Wirtz, T., Blank, L.M., Hornef, M., von Bergen, M., et al. (2022). A physiologically based model of bile acid metabolism in mice. Preprint at bioRxiv. eprint. https://doi.org/10.1101/2022.11.10.515857. https://www.biorxiv.org/content/early/2022/11/13/2022.11.10.515857.full.pdf.
85. Klindworth, A., Pruesse, E., Schweer, T., Peplies, J., Quast, C., Horn, M., and Glöckner, F.O. (2013). Evaluation of general 16S ribosomal RNA gene PCR primers for classical and next-generation sequencing-based diversity studies." eng. Nucleic Acids Res. *41*, e1.
86. Edgar, R.C. (2013). "UPARSE: highly accurate OTU sequences from microbial amplicon reads." eng. Nat. Methods *10*, 996–998.
87. Edgar, R.C. (2010). Search and clustering orders of magnitude faster than BLAST. Bioinformatics *26*, 2460–2461.
88. Pruesse, E., Peplies, J., and Glöckner, F.O. (2012). SINA: accurate high-throughput multiple sequence alignment of ribosomal RNA genes. Bioinformatics *28*, 1823–1829.
89. Lagkouvardos, I., Fischer, S., Kumar, N., and Clavel, T. (2017). Rhea: a transparent and modular R pipeline for microbial profiling based on 16S rRNA gene amplicons. PeerJ *5*, e2836.
90. Pham, H.T., Arnhard, K., Asad, Y.J., Deng, L., Felder, T.K., St John-Williams, L., Kaever, V., Leadley, M., Mitro, N., Muccio, S., et al. (2016). Inter-Laboratory Robustness of Next-Generation Bile Acid Study in Mice and Humans: International Ring Trial Involving 12 Laboratories. J. Appl. Lab. Med. *1.2*, 129–142. https://doi.org/10.1373/jalm.2016.020537.
91. Godon, J.J., Zumstein, E., Dabert, P., Habouzit, F., and Moletta, R. (1997). Molecular microbial diversity of an anaerobic digestor as determined by small-subunit rDNA sequence analysis." eng. Appl. Environ. Microbiol. *63*, 2802–2813.
92. Berry, D., Ben Mahfoudh, K., Wagner, M., and Loy, A. (2011). Barcoded primers used in multiplex amplicon pyrosequencing bias amplification." eng. In. Appl. Environ. Microbiol. *77*, 7846–7849.
93. Lagkouvardos, I., Kläring, K., Heinzmann, S.S., Platz, S., Scholz, B., Engel, K.H., Schmitt-Kopplin, P., Haller, D., Rohn, S., Skurk, T., and Clavel, T. (2015). Gut metabolites and bacterial community networks during a pilot intervention study with flaxseeds in healthy adult men. Mol. Nutr. Food Res. *59*, 1614–1628.
94. Lagkouvardos, I., Joseph, D., Kapfhammer, M., Giritli, S., Horn, M., Haller, D., and Clavel, T. (2016). IMNGS: A comprehensive open resource of processed 16S rRNA microbial profiles for ecology and diversity studies. Sci. Rep. *6.1*, 33721. https://doi.org/10.1038/srep33721.
95. Charlier, F., et al. (2022). Statannotations. Version v0.5. https://doi.org/10.5281/zenodo.7213391.

## STAR★METHODS

### KEY RESOURCES TABLE

| REAGENT or RESOURCE | SOURCE | IDENTIFIER |
|---|---|---|
| **Biological samples** | | |
| Tissue samples from duodenum, jejunum, ileum, proximal and distal colon | C57BL/6J (WT*; SPF**)<br>C57BL/6N (WT*; GF***) from ILAS, University Hospital RWTH Aachen | –<br>* WT = wild type<br>** SPF = specific pathogen free<br>*** GF = germ free |
| **Chemicals, peptides, and recombinant proteins** | | |
| 2-Propanol, ROTIPURAN® ≥ 99.8% | Carl Roth GmbH + Co. KG, Karlsruhe Germany | 6752.4 |
| 5X Reaction Buffer for RT | Thermo Fisher Scientific, Waltham, Massachusetts, USA | EP0442 |
| ABsolute qPCR Mix, ROX | Thermo Fisher Scientific, Waltham, Massachusetts, USA | AB1138B |
| Aqua ad iniectabilia (nuclease-free) | B. Braun SE, Melsungen, Germany | 2351744 |
| Ethanol, ROTISOLV® | Carl Roth GmbH + Co. KG, Karlsruhe Germany | P076.1 |
| 7TRIzol™ Reagent | Merck & Co. Inc., Kenilworth, New Jersey, USA. | 15596026 |
| Tirchlormethan/Chloroform 2.5 L ROTISOLV® HPLC | Carl Roth GmbH + Co. KG, Karlsruhe, Germany | 7331.2 |
| *Polyvinylpyrrolidone* | *Merck* | *Cat#7443* |
| *AMPure XP beads* | *Beckman Coulter* | *Cat#A63881* |
| *Guanidine Thiocyanate* | *Sigma-Aldrich* | *Cat#G9277* |
| *N-Lauroylsarcosine Sodium Salt* | *Sigma-Aldrich* | *Cat#61743* |
| *Zirconia beads* | *Carl Roth* | *Cat#110791012* |
| *Stool DNA Stabilizer* | *Stratec biomedical* | *Cat#1038111100* |
| *Rnase* | *VWR* | *Cat#E866* |
| *Phusion® High-Fidelity DNA Polymerase Hotstart* | *Thermo Scientific* | *Cat#F549L* |
| *BioReagent Dimethyl sulfoxide (DMSO), Molecular Biology Grade, Liquid, ≥99.9%* | *Sigma-Aldrich* | *Cat#D8418* |
| Bile Acid Kit | Biocrates | 20813 |
| Acetonoitril hypergrade für LC-MS | Merck | 1000292500 |
| Methanol LC-MS Chromasolv | Honeywell | 34966-2.5L |
| Ameisensäure | Honeywell | 56302-50ML |
| 2-Propanol gradient grade für die Flüssigkeitschromatographie LiChrosolv | Merck | 1010402500 |
| **Critical commercial assays** | | |
| MiSeq Reagent Kit v3 (600-cycle) | Illumina | Cat#MS-102-3003 |
| NucleoSpin® gDNA Clean-up | Macherey-Nagel | Cat#740230.250 |
| Quant-it PicoGreen dsDNA Assay | Invitrogen | Cat#P7589 |
| **Deposited data** | | |
| raw amplicon sequencing data | This paper | ENA: PRJEB58856 |

(*Continued on next page*)

*Continued*

| REAGENT or RESOURCE | SOURCE | IDENTIFIER |
|---|---|---|
| Experimental models: Organisms/strains | | |
| Mouse: C57BL/6N | Internal breeding colony (RWTH Aachen) | N/A |
| Oligonucleotides | | |
| dNTP Set 100 mM Solutions | Thermo Fisher Scientific, Waltham, Massachusetts, USA | R0181 |
| Oligo (dT) Primer (50 μM) | Thermo Fisher Scientific, Waltham, Massachusetts, USA | AM5730G |
| 341F-ovh | Merck | 5′-TCGTCGGCAGCGTCAGATGTGTATA AGAGACAG CCTACGGGNGGCWGCAG-3′ |
| 785r-ovh | Merck | 5′-GTCTCGTGGGCTCGGAGATGTGTAT AAGAGACAG GACTACHVGGGTATCTAATCC-3′ |
| SC501 341-ovh-HTS- | Merck | 5′-AATGATACGGCGACCACCGAGATCTACAC ACGACGTGTCGTCGGCAGCGTC-3′ |
| SA701 785r-ovh-HTS- | Merck | 5′-CAAGCAGAAGACGGCATACGAGAT AACTCTCGGTCTCGTGGGCTCGG-3′ |
| Software and algorithms | | |
| CFX manager software Version 3.1 | Bio-Rad, Hercules, California, USA | https://www.bio-rad.com/ |
| Graph Pad Prism Version 7 | GraphPad Software Inc., San Diego, California, USA | https://www.graphpad.com/ |
| Open Systems Pharmacology Suite Version 11.150 | Open Systems Pharmacology Community | https://www.open-systems-pharmacology.org/ |
| Integrated Microbial Next Generation Sequencing platform | Lagkouvardos et al.[85] | www.imngs.org |
| USEARCH 11.0 | Edgar et al.[86] | http://www.drive5.com/usearch/ |
| SINA 1.6.1 (taxonomy of SILVA release 138) | Pruesse et al.[87] | https://bioconda.github.io/recipes/sina/README.html |
| Rhea pipeline | Lagkouvardos et al.[88] | https://lagkouvardos.github.io/Rhea |
| Statannotations package | Charlier et al.[89] | https://github.com/trevismd/statannotations |
| Other | | |
| γ-irradiated standard chow | ssniff Spezialdiäten GmbH | V1124-927 |
| autoclaved standard chow | ssniff Spezialdiäten GmbH | V1124-300 |
| RevertAid | Thermo Fisher Scientific, Waltham, Massachusetts, USA | EP0442 |
| RiboLock RNase-Inhibitor | Thermo Fisher Scientific, Waltham, Massachusetts, USA | EO0381 |
| Taqman Probe OST-A (gene: Slc51a) | Thermo Fisher Scientific, Waltham, Massachusetts, USA | Mm00521530_m1 |
| Taqman Probe OST-B (gene: Slc51b) | Thermo Fisher Scientific, Waltham, Massachusetts, USA | Mm01175040_m1 |
| Taqman Probe ASBT (gene: Slc10a2) | Thermo Fisher Scientific, Waltham, Massachusetts, USA | Mm00488258_m1 |
| Taqman Probe Hmbs (gene: hmbs) | Thermo Fisher Scientific, Waltham, Massachusetts, USA | Mm01143545_m1 |

## RESOURCE AVAILABILITY

### Lead contact

Further information and requests for resources and reagents should be directed to and will be fulfilled by the lead contact, Lars Kuepfer (lkuepfer@ukaachen.de)

### Materials availability

This study did not generate new unique reagents.

### Data and code availability

The raw amplicon sequencing data generated in the context of this study have been submitted to the European Nucleotide Archive and are publicly available under project accession number ENA: PRJEB58856. The computational model file is available on http://www.ukaachen.de/kuepfer. Any additional information required to reanalyze the data reported in this paper is available from the lead contact upon request.

## EXPERIMENTAL MODEL AND STUDY PARTICIPANT DETAILS

### Mouse housing conditions and sampling

Samples were collected from both male and female (50% female) germ-free (GF) and specific-pathogen free (SPF) C57BL/6N mice euthanized for scientific procedures in accordance with the German Animal Protection Law (TierSchG). The internal animal care and use committee (IACUC) at the University Hospital of RWTH Aachen approved the collection of gut content, body fluids, and organs from donor mice not subjected to any experimental treatment (internal approval no. 70018A4). GF mice were housed in isolators (NKPisotec, Flexible film isolator type 2D) under sterile conditions. To obtain SPF mice with C57BL/6N background, mice were taken from the isolator and colonised passively with a complex microbiota by cohousing with SPF mice. Mice of the first generations of C57BL/6N SPF mice after breeding were sampled for this work. Room temperature was kept between 21°C and 24°C and 25–40% humidity on a 12h:12h day:night cycle. All mice were fed a standard chow *ad libitum* (GF mice: γ-irradiated standard chow, V1124-927; SPF mice: autoclaved standard chow, ssniff V1124-300) and given autoclaved tap water (pH 7). Mice were housed in single sex cages with Tek-Fresh bedding (ENVIGO). Fecal samples of GF mice were taken to confirm the GF status via microscopic observation after Gram-staining and plating on both anaerobic and aerobic agar plates. Mice were sacrificed in the afternoon (3–6 p.m.) with free access to food at an age of 12- to 13-week and blood, urine, gut tissue and content, liver, gall bladder and kidneys were collected. Systemic blood was collected from vena cava, put on ice for 5–10 min and subsequently centrifuged at 4,500 rpm for 15 min to obtain serum. The small intestine was divided by length into duodenum (proximal 16%), jejunum (middle 74%), and ileum (distal 10%). The colon was divided in proximal (50%) and distal (50%) parts. All samples got frozen immediately and stored at −80°C.

## METHOD DETAILS

### Bile acid measurements

#### *Sample preparation*

First, x mg solid matrix were mixed with five times the µl amount of ACN:water (1:1, v/v) and homogenised with a TissueLyser II (30 Hz, 10 min; Retsch Qiagen). After a short centrifugation (2 min, 14000 rpm) 100 µL of the supernatant were added to 500 µL ACN:water:methanol (3:1:2, v/v/v) and the sample was vortexed for 5 min. After sonication (5 min) and centrifugation (14,000 rpm, 4°C, 5 min), 550 µL of the supernatant was transferred to a new tube and evaporated to dryness. The pellet was reconstituted in 100 µL 50% and 10 µL was used for analysis. For serum samples, 10 µL samples were used.

#### *LC-MS analysis*

The analysis was performed using the validated Bile Acid Kit (Biocrates Life Sciences, Innsbruck, Austria) as described in Pham et al.[90] For that 10 µL of the native samples/sample extract were pipetted onto a 96 well sandwich filter plate and prepared according to manufacturer's instructions. For quantitation, 7 external calibration standards (each containing all 19 bile acids) and 10 isotope-labeled internal standards are used. A detailed list of metabolites is available at the manufacturer's homepage Kit (Biocrates Life Sciences AG, Innsbruck, Austria). The LC-MS/MS analysis carried out by MRM acquisition using a Waters Acquity UPLC System coupled with QTRAP 5500 (AB Sciex, Concord, Canada). MP A consisted of 10 mM ammonium acetate and 0.015% formic acid, while MP B was of a mixture of acetonitrile/methanol/water (65/30/5; v/v:v), 10 mM ammonium acetate and 0.015% formic acid. Data processing is carried out with the provided quantitation method Kit (Biocrates Life Sciences AG, Innsbruck, Austria).

#### *Bile acid transporter expression*

RNA isolation from homogenized tissue samples were performed using TRIzol reagent. Tissue homogenization was done using the FastPrep-24TM 5G from MP BiomedicalsTM. Isolated RNA was transcribed into cDNA using ReverseAid (Thermo Fisher) and RiboLock Inhibitor (Thermo Fisher). Quantitative PCR was done based on the use of taqman probes (Thermo Fisher) for the respective gene of interest (GOI). GOI expression was normalized to the expression of a housekeeping gene.

## Microbiota analysis by high-throughput sequencing

### *Isolation of metagenomic DNA*

For DNA isolation a modified protocol according to Godon et al.[91] was used. Frozen samples were mixed with 600 µL stool DNA stabilizer (Stratec biomedical) and thawed at room temperature. After transfer to autoclaved 2-mL screw-cap tubes containing 500 mg of 0.1 mm-diameter silica/zirconia beads, 250 µL 4 M guanidine thiocyanate in 0.1 M Tris (pH 7.5) and 500 µL 5% N-lauroyl sarcosine in 0.1 M PBS (pH 8.0) were added. Samples were incubated at 70°C and 700 rpm for 60 min. The cell disruption on a FastPrep instrument (MP Biomedicals) fitted with a 24 × 2 mL cooling adaptor filled with dry ice was conducted 40 s at 6.5 M/s for 3 times. An amount of 15 mg Polyvinylpyrrolidone (PVPP) was added and samples were vortexed, followed by 3 min centrifugation at 15.000 x g and 4°C. Approximately 650 µL of the supernatant were transferred into a new 2 mL tube, which was centrifuged for 3 min at 15.000 x g and 4°C. Of the supernatant 500 µL were transferred into a new 2 mL tube and 50 µg of RNase were added before incubating for 20 min at 37°C and 700 rpm. Subsequently gDNA was isolated using the NucleoSpin gDNA Clean-up Kit from Macherey-Nagel according to the manufacturer's protocol. DNA was eluted from columns twice using 40 µL Elution buffer and concentration was measured with NanoDrop (Thermo Scientific). Samples were stored at −20°C.

### *Illumina sequencing of 16S rRNA gene amplicons*

Library preparation and sequencing were performed as described in detail previously Lagkouvardos2015 using an automation platform (Biomek400, Beckman Coulter). Briefly, the V3-V4 region of 16S rRNA genes was amplified in duplicates (25 cycles) following a two-step protocol[92] using primers 341F-785R.[85] The AMPure XP system (Beckman Coulter) was used for purification before sequencing was carried out with pooled samples in paired-end modus (PE300) on a MiSeq system (Illumina, Inc.) with 25% (v/v) PhiX standard library according to the manufacturer's instructions.

## Computational methods

### *PBPK modeling*

Physiologically-based pharmacokinetic (PBPK) models describe the physiology of an organism at a large level of detail. Organs are explicitly represented in PBPK models and they are linked through systemic vascular circulation. Tissue concentrations can be simulated in PBPK models, even if they are experimentally inaccessible. Parameters in PBPK models explicitly represent specific physiological functions and they are taken from previously curated collections of parameters including organ volumes, surface areas, tissue composition and blood perfusion rates, respectively. For that reason, identification of PBPK models is limited to very few parameters, usually related to active processes underlying compound distribution of as well as elimination. PBPK models are hence based on a large amount of prior knowledge including detailed description of physiological processes such as enterohepatic circulation or absorption in the intestine.

### *Kinetic rate laws*

Describing BA synthesis, a constant flux within the intracellular space of the liver was assumed. The following rate law was applied in mice:

$$v_{synth} = s_{GF} * s_{sex} * EM * k_{synth}$$

where $s_{GF}$ and $s_{sex}$ represent scaling factors adjusting the overall activity between SPF and GF as well as male and female mice, $EM$ the amount of catalyzing enzyme and $k_{synth}$ the absolute synthesis rate. For the remaining enzymatic reactions and transport processes, Michaelis-Menten kinetics were applied, following in mice:

$$v = s_{GF} * s_{sex} * EM * k_{cat} * K_{water} * C / (K_m + K_{water} * C)$$

with $K_{water}$ describing the partition coefficient of the BA between water and the source compartment of the BA, $K_m$ the Michaelis-Menten constant and $C$ the BA concentration in the source compartment. $k_cat$ represents the number of substrate BA each enzyme site converts to product per unit time, and in which the enzyme is working at maximum efficiency and is calculated as

$$k_{cat} = v_{max}/C_{ref}$$

with $v_{max}$ being the maximum rate of reaction and $C_{ref}$ the enzyme reference concentration of 1 µM. For renal excretion, tubular excretion with Michaelis-Menten kinetic was selected within PKSim:

$$v = fu * TS_{max} * C_{kid-pls} / (K_m + fu * C_{kid-pls})$$

with $TS_{max}$ describes the intrinsic maximum rate for tubular secretion, fu the fraction unbound BA in blood plasma and $C_{kid-pls}$ the BA concentration within the plasma sub-compartment of the kidney.

### *Calculations*

Parameter fitting was performed with the Monte Carlo algorithm implemented in the Open Systems Pharmacology suite. Residual calculation was set to linear and weights were derived from measured SD. Sensitivity analysis was performed using the default settings within MoBi. For sensitivity coefficients a threshold of 1 and -1 in either the male or female model was applied. Most reactions were defined as simple Michaelis-Menten kinetics, for BA synthesis a constant flux was assumed. For assessment of impaired gut barrier function, unperturbed

paracellular permeability of BAs was set to their corresponding transcellular permeability calculated by MoBi on basis of their physicochemical properties.

### *16S rRNA amplicon data analysis*

Data was analyzed with an updated version of a workflow previously described by Lagkouvardos et al.[93] Raw reads were processed using the Integrated Microbial Next Generation Sequencing platform (www.imngs.org)[94] based on UPARSE.[86] For this, sequences were demultiplexed and trimmed to the first base with a quality score of at least 10. Subsequent pairing, chimera filtering as well as OTU clustering (97% identity) was performed using USEARCH 11.0.[87] Sequences that had less than 350 and more than 500 nucleotides and paired reads with an expected error above 2 were excluded from further analysis. To avoid GC bias and non-random base composition, remaining reads were trimmed by fifteen nucleotides on each end. Clustering of operational taxonomic units (OTUs) was done at 97% sequence similarity. For further analysis, only those with a relative abundance above 0.25% in at least one sample were kept. Sequence alignment and taxonomic classification was done with SINA 1.6.1, applying the taxonomy of SILVA release 138.[88]

For assessment of microbial richness, diversity and community structure, the Rhea pipeline was used.[89] A detailed description of statistical tests applied are provided in the Rhea support information and in the corresponding scripts (https://lagkouvardos.github.io/Rhea). Normalization of sequence counts was done via simple division to their sample size and then multiplication by the size of the smaller sample before subsequent calculation of alpha-diversity parameters. Beta-diversity analyses were based on the calculation of unweighted and generalized UniFrac distances.[25,25]

## QUANTIFICATION AND STATISTICAL ANALYSIS

The PBPK model of bile acid metabolism was established in PK-Sim and further reactions and adjustments were done in MoBi (Open Systems Pharmacology suite Version 11.150). Model simulations were performed using the ospsuite-R package in R (version 11.0.123). Plotting and statistical testing was done with custom Python scripts. Where applicable, p value correction for multiple testing was done using Benjamini-Hochberg correction using the statannotations package.[95] For assessment of impaired gut barrier function, unperturbed paracellular permeability of BAs was set to their corresponding transcellular permeability calculated by MoBi on basis of their physicochemical properties.